Author Manuscript

Evidence for the Neoproterozoic rifting of Rodinia in the Rocky Mountain Front Range

Kendra E. Murray[1,2], Nathan A. Niemi[2], Marin K. Clark[2]

[1]Department of Geosciences, Idaho State University, 921 S. 8th Ave., Pocatello, ID 83209.

[2]Department of Earth and Environmental Sciences, University of Michigan, 1100 N. University Ave., Ann Arbor, MI 48109.

Corresponding author: Kendra E. Murray (kendramurray@isu.edu)

Key Points:

- Zircon U-Th/He thermochronology supports that the Rocky Mountain Front Range is an inverted Neoproterozoic extensional basin
- Sensitivity testing reveals the reasons this history is resolved and offers insights for future deep-time thermal history modeling
- The Neoproterozoic-Paleozoic timing of post-rifting exhumation is too poorly constrained to resolve tectonic vs. glacial drivers

Keywords: "deep-time thermochronology", "thermal history modeling", "Rodinia rifting", "Neoproterozoic", "Rocky Mountains"

This is the author manuscript accepted for publication and has undergone full peer review but has not been through the copyediting, typesetting, pagination and proofreading process, which may lead to differences between this version and the Version of Record. Please cite this article as doi: 10.1029/2023TC008216.

This article is protected by copyright. All rights reserved.

Author Manuscript

Abstract

Recent advances in low-temperature thermochronology enable the recovery of deep-time thermal histories from Precambrian crystalline rocks shaped by multiple tectonic events, offering unprecedented opportunities to test tectonic hypotheses and links to significant biologic and climatic episodes. In particular, the late Neoproterozoic breakup of supercontinent Rodinia profoundly shaped the western margin of Laurentia, leaving a geologic record along the Cordilleran hingeline that temporally associates continental rifting with biological change at the Ediacaran-Cambrian transition and may explain the unusual eastern extent of the Laramide orogeny. However, sedimentary evidence east of the Cordilleran hingeline is lacking, leaving postulated links untested. Here we interpret Neoproterozoic to recent tectonic histories from the Colorado Front Range using thermal history modeling of zircon (U-Th)/He (ZHe) ages (50-607 Ma), which vary with grain U-Th composition. These models are constrained by geologic records that place basement rocks near Earth's surface at ca. 700, 500, and 300 Ma, and they resolve late Neoproterozoic heating to 240-285°C followed by cooling. Sensitivity tests confirm this heating signal depends on fitting Mesoproterozoic $^{40}Ar/^{39}Ar$ ages and a ZHe dataset that includes high-U-Th grains with reproducible 61±7.5 Ma ages that correspond to Colorado Mineral Belt magmatism and Laramide exhumation. We interpret the Neoproterozoic heating as direct evidence that intracontinental rifting in the Front Range region drove kilometer-scale burial coeval with global glaciation and the fragmentation of Rodinia. Although the magnitude and duration of reheating are well constrained, resolving subsequent cooling during Neoproterozoic-Paleozoic time strongly depends on surface constraints from the geologic record.

1 Introduction

Resolving the influence of Proterozoic tectonic events on contemporaneous and later geologic, climatic, and biological processes requires robustly quantifying their timing and spatial extent. However, geologic evidence for ancient tectonic events is commonly sparse and poorly constrained due to the immense magnitude of Proterozoic time and poor preservation of ancient geologic records. The low-temperature (<300˚C) thermal record of Precambrian (i.e., 'deep-time') events—as preserved in the crystalline basement rocks that experienced heating and cooling due to processes such as burial and exhumation—has recently become accessible through advances in thermochronology (McDannell & Flowers, 2020) , in particular the application of the zircon (U-Th)/He (ZHe) system (Guenthner et al., 2013; Reiners, 2005) . Application of these methods are making great strides at understanding the connections between major tectonic, biologic and climatic signals during one of the most enigmatic periods of Earth's history, and the Cordillera of the western United States preserves perhaps one of the most complete and compelling stratigraphic records of these interconnections (Witkosky & Wernicke, 2018) .

The Neoproterozoic break-up of the supercontinent Rodinia left an indelible mark on the geologic and tectonic evolution of the western margin of Laurentia. The edge of the cratonic margin that developed during this rifting (the "Cordilleran hingeline") demarcates the extent of

This article is protected by copyright. All rights reserved.

significant Neoproterozoic and Paleozoic syn- and post-rifting sedimentation, separates Mesozoic Sevier and Laramide-style compressional deformation, and traces the easternmost-extent of Cenozoic Basin and Range extension (Picha & Gibson, 1985) . The cratonic edge of Laurentia defines the preservation limit of Neoproterozoic strata associated with the rifting of Rodinia, which are presently exposed from the Uinta Mountains in Utah to western Nevada and eastern California (Stewart, 1970) but are absent to the east in Colorado and the mid-continent. These strata preserve evidence of multiple Neoproterozoic glaciations attributed to Snowball Earth-like conditions (Corsetti & Grotzinger, 2005; Hoffman et al., 2017; Prave, 1999; Wang et al., 2023). The stratigraphic record of glaciations is associated with major carbon isotopic excursions (e.g., Kaufman et al., 2007) , as well as the Ediacaran-Cambrian transition to complex life forms (Peters & Gaines, 2012; E. F. Smith et al., 2022; Witkosky & Wernicke, 2018). Evolutionary diversification during Neoproterozoic time has been directly attributed to continental rifting and supercontinent break-up (e.g., Plummer, 2024), although other environmental triggers are also postulated (E. F. Smith et al., 2022). The glaciations preserved in the stratigraphic record have also been posited to be associated with a Neoproterozoic continental denudation event of remarkable scale (e.g., Keller et al., 2019).

The cratonic edge of Laurentia during Mesozoic time delineated the boundary between thin-skinned thrusting associated with the Sevier orogenic belt and the thick-skinned thrusting associated with the Laramide orogeny (e.g., Yonkee & Weil, 2015). The discontinuous nature of Laramide structures, and their significant variation in orientation with respect to the regional stress field, has led to the inference that Laramide structures are associated with pre-existing crustal weaknesses, including faults and shear zones associated with pre-Mesozoic orogenic events (e.g., Weil & Yonkee, 2023). Within the Southern Rocky Mountains, the distribution of Laramide fault-bounded uplifts has been suggested to reflect the inversion of Neoproterozoic extensional systems that accommodated supercontinent rifting (Figs. 1a, b; Chapin et al., 2014; Marshak et al., 2000; Marshak & Paulsen, 1996) based on similarities between Laramide fault geometries and those of recognized inverted rifts and the potential of the inversion hypothesis to thereby explain the pattern of Laramide deformation (Marshak et al., 2000). However, this linkage is challenged by the lack of stratigraphic evidence of the Proterozoic history of the Southern Rocky Mountains, which is presumed to have been removed through multiple episodes of Phanerozoic tectonism. Evidence for Neoproterozoic rifting along the Colorado range front and later reactivation by Laramide compressional structures along the eastern front of the Southern Rocky Mountains would in part explain the enigmatic and unusual extent of shortening deformation so far into the continental interior during eastward subduction of the Farallon-Pacific plate during Late Cretaceous time.

In short, understanding key aspects of the Neoproterozoic to present geologic, climatic, and biologic evolution of western Laurentia depends on connecting events recorded through the deposition and deformation of strata on the extended margin of Rodinia to the tectonic evolution of the craton itself; however, the paucity of Neoproterozoic strata preserved on the craton offers limited opportunity to forge these connections. Published deep-time thermal histories provide a

This article is protected by copyright. All rights reserved.

Author Manuscript

pathway to approach these challenges, and Proterozoic rocks from the Front Range of Colorado (Figs. 1b, 2a) have taken center-stage in attempts to unravel deep-time thermal histories that illuminate the Neoproterozoic evolution of western North America.

Published deep-time thermal history analyses of zircon (U-Th)/He (ZHe) data from the Front Range (Fig. 2), the largest of the Laramide ranges, have been central to an ongoing debate about the significance of the Great Unconformity (GU) (e.g., Keller et al., 2019), a typically >1 Gyr gap in the rock record that limits our understanding of the Proterozoic Earth. This debate hinges on whether Proterozoic cooling of basement rocks below the GU documents regional exhumation related to the protracted amalgamation and/or break-up of the supercontinent Rodinia (Flowers et al., 2020; Havranek & Flowers, 2022; Ricketts et al., 2021) or global Cryogenian erosional exhumation during "Snowball Earth" glaciations (McDannell et al., 2022b). However, various published studies that interpret the Proterozoic thermal history of the basement rocks in the Front Range region (Flowers et al., 2020; Havranek & Flowers, 2022; Ricketts et al., 2021; McDannell et al., 2022b) report different, and in some cases contradictory, Neoproterozoic thermal histories. These differences likely depend on several factors, including the degree of preservation of Proterozoic thermal histories in specific suite of samples, true spatial variability in Proterozoic thermal histories, and model design and data handling choices (Flowers et al., 2022; McDannell et al., 2022a, 2022b). The significance of these differences must be determined in order to advance our knowledge of the Proterozoic Earth using deep-time thermochronology.

Here, we present thermal history models of ZHe data, sensitivity analyses integrated with previously published model results (Murray, Stevens Goddard, et al., 2022), and zircon U/Pb data, and we resolve a distinctive late Neoproterozoic heating event in the central Front Range (Fig. 2a). We evaluate how variable preservation of Proterozoic thermal information and model design choices manifest in the thermal history results. In addition to discussing the geologic implications of our findings, we consider what new information about Proterozoic events (i.e., their timing, magnitude, etc.) appears to be most unambiguously and quantitively resolved by this thermal history analysis, with the intention of looking ahead to the emerging opportunities and limitations of studies that leverage thermochronologic datasets to advance our understanding of Proterozoic tectonics.

Author Manuscript

This article is protected by copyright. All rights reserved.

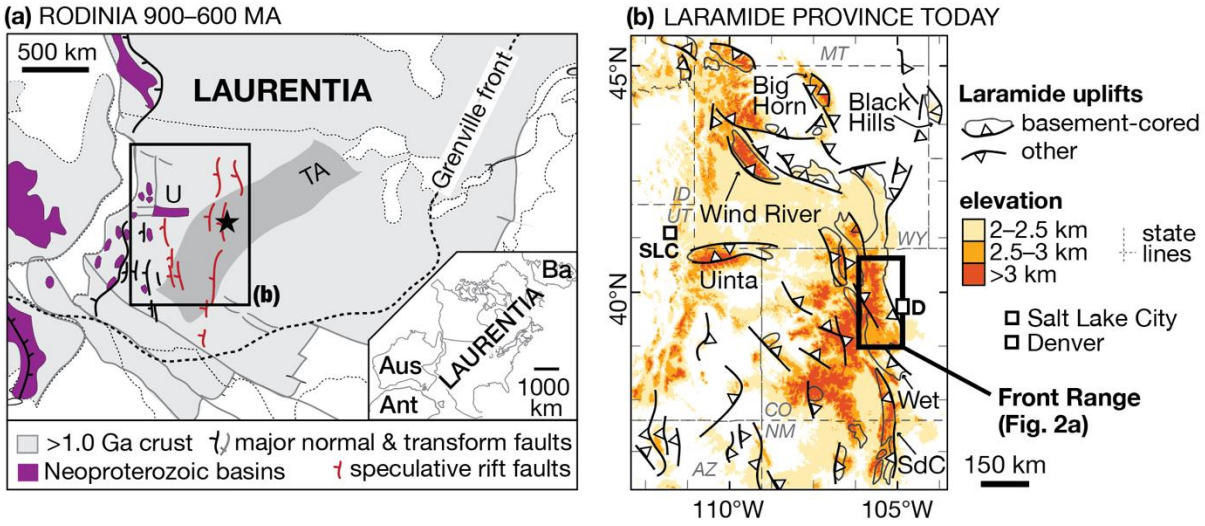


Figure 1. (a) *A Neoproterozoic plate reconstruction of supercontinent Rodinia during rifting and early breakup, modified from Karlstrom et al.* (1999)*. Coeval sedimentary basins west of the Uinta Mountains (U) document this protracted rifting event but are absent on the craton to the east. Black star indicates the location of this study. TA—Transcontinental Arch location from Carlson* (1999)*. Ba—Baltica, Aus—Australia, Ant—Antarctica.* ***(b)*** *The fault-blocks uplifted during the Late Cretaceous–Eocene Laramide Orogeny* (modified from Marshak et al., 2000) *overlaid on modern topography.*

2 Geologic history of the central Front Range

The geology of the central Front Range is dominated by Proterozoic plutonic and metamorphic rocks (Cole & Braddock, 2009; Kellogg et al., 2008)The Proterozoic samples in our study are from ca. 1.7 Ga granodiorites (Premo & Fanning, 2000) and surrounding Paleoproterozoic orthogneisses (Fig. 2a). Mesoproterozoic hornblende $^{40}Ar/^{39}Ar$ ages document that these Paleoproterozoic rocks cooled below ~450 ˚C after a period of regional magmatism at ca. 1.4 Ga (Shaw et al., 1999), suggesting that they have been in the low-temperature thermal window since that time.

Sparse exposures of Neoproterozoic rocks that formed near Earth's surface provide two key geologic constraints on the thermal history of the central Front Range: (1) they place the crystalline rocks sampled for this study in the near surface at that time and (2) they provide an upper limit on the magnitude of basement erosion since late Neoproterozoic time. One surface datum is defined by the Green Mountain kimberlite diatreme (Fig. 3a), which has 800-500 Ma phlogopite $^{40}Ar/^{39}Ar$ ages and a Sm/Nd isochron age of 572±59 Ma (Lester et al., 2001), consistent with an absence of Paleozoic xenoliths. A second surface datum is defined by the Tavakaiv (Tava) quartzites, which are rare clastic bodies (Cross, 1894) found throughout the Front Range region (Fig. 2a; Fig. 3), with features that suggest forceful emplacement of sand-

This article is protected by copyright. All rights reserved.

Author Manuscript

rich fluids into the crystalline rocks (Courtney-Davies et al., 2024; Flowers et al., 2020; Siddoway et al., 2013, 2019; Siddoway & Gehrels, 2014). Sedimentary and structural features in the Tava, as in other injected, unlithified sand bodies, imply injection at depths of no more than 0.5–1 km (Hurst et al., 2011; Jonk, 2010; Jonk et al., 2004). Thus, the presence of the Tava bodies indicates that the rocks that host them were near Earth's surface at the time of Tava emplacement; the preservation of these sand bodies further precludes significant erosion of crystalline basement since their emplacement. A Neoproterozoic formation age for the Tava injectities, including in our study area (Fig. S1, Table S3), is supported by detrital zircon U/Pb ages, which correlate the Tava sandstones to sedimentary rocks deposited in western Laurentia ca. 800-680 Ma (Jensen et al., 2018; Siddoway & Gehrels, 2014). U/Pb geochronology of hematite veins that cross-cut Tava bodies are consistent with this age range and constrain sand injectite emplacement to ~690-660 Ma (Courtney-Davies et al., 2024). Hematite (U-Th)/He analysis in the Williams Fork Range suggest a maximum age of Tava sand emplacement at 676±26 Ma (Jensen et al., 2018).

The deposition of variably preserved Phanerozoic sedimentary rocks also provides a suite of paleosurface datums throughout Paleozoic and Mesozoic time. Deposition of the late Cambrian Sawatch Formation on crystalline basement rocks in the southern Front Range (Fig. 2a; Siddoway et al., 2013) and surrounding regions (Tweto, 1979) places crystalline basement rocks at the surface ca. 500 Ma, while the overlying Ordovician and Mississippian strata document no more than 1 km of net burial prior to Carboniferous time. Regionally extensive conglomeratic facies of the Pennsylvanian Fountain Formation (Howard, 1966; Sweet et al., 2015) document exhumation and erosion of Front Range basement rocks during the Ancestral Rocky Mountains (ARM) orogeny ca. 320-280 Ma (Kluth and Coney, 1981; Leary et al., 2017). The Fountain Formation was deposited on a nonconformity surface developed on crystalline basement (Figs. 2a, 3); this nonconformity may be a composite surface that previously experienced early Paleozoic erosion and subsequent burial, but which nonetheless requires crystalline basement rock to be at the surface during Fountain Formation deposition. In our study area, post-ARM burial is documented by Permian and Mesozoic strata preserved in the Denver Basin east of Boulder (Fig. 3; Wrucke & Wilson, 1967). These strata document ~700-1000 m net burial of the crystalline basement by the end of deposition of the Niobrara Formation at 82 Ma, followed by an additional ~2500 m of burial by the marine Pierre Shale by ca. 68 Ma. The depositional age of the Pierre Shale is known from ammonite biozones (Kauffman, 1977), which support that ~50 % of the total thickness (~1300 m) was rapidly deposited between 69 and 68 Ma (Fig. S2).

The end of Pierre Shale deposition in latest Cretaceous time marks the transition from marine to synorogenic sedimentation at the onset of Laramide tectonism in the Front Range region (Lawton, 2008; Raynolds, 1997; Weimer, 1973) and was accompanied by magmatism and activation of compressional structures (e.g., Nesse, 2006). Colorado Mineral Belt (CMB) magmas were emplaced into the crystalline basement rocks in the central Front Range during the latest Cretaceous to Paleogene (Chapin, 2012). The CMB is a NE-trending 15-50 km wide

This article is protected by copyright. All rights reserved.

Author Manuscript

lineament of small-volume plutons and stocks that is associated with polymetallic ore deposits (Figs. 2a, 3; Chapin, 2012; Lovering & Goddard, 1950). The orientation of the CMB has been hypothesized to follow a system of Proterozoic shear zones (Caine et al., 2006, 2010; McCoy et al., 2005; Tweto & Sims, 1963). The sequential erosion of the volcanic components of the CMB, followed by Phanerozoic sedimentary and then Proterozoic crystalline basement rocks, is documented in a complete Front Range unroofing sequence in synorogenic strata in the Denver Basin (Kelley, 2002).

Author Manuscript

This article is protected by copyright. All rights reserved.

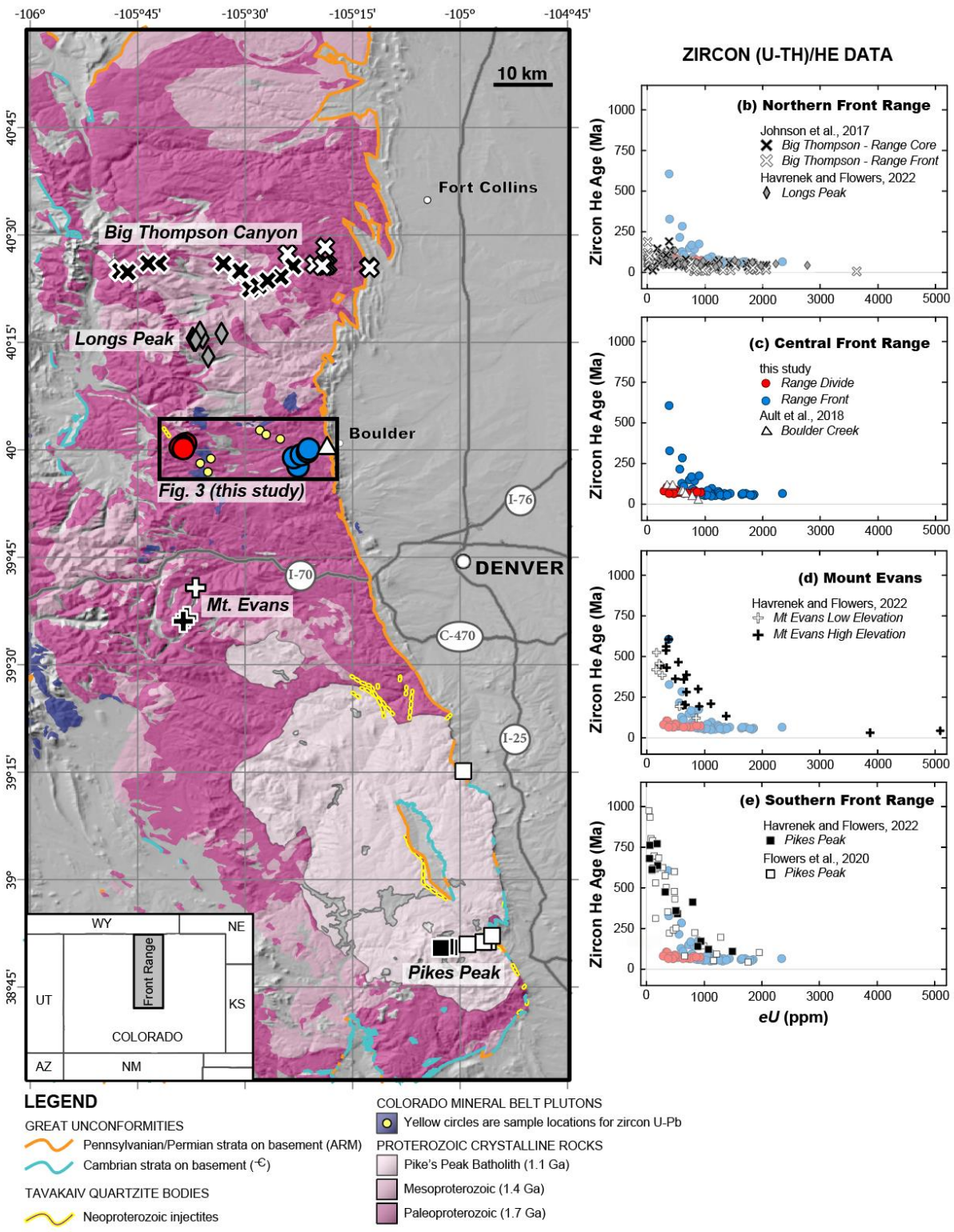


Figure 2. (a) *Simplified geologic map of the crystalline rocks in the Front Range, the unconformable contacts between Proterozoic basement rocks and Cambrian (Є) sediments or the late Paleozoic sediments deposited during the Ancestral Rocky Mountains (ARM) orogen* (G.

This article is protected by copyright. All rights reserved.

N. Green, 1992), *and the Tavakaiv injectite localities* (Cole & Braddock, 2009; Kellogg et al., 2008; Siddoway & Gehrels, 2014). *Symbols indicate sample locations for this study* (Murray, Niemi, et al., 2022), *which are from the Paleoproterozoic basement rocks, and other published zircon (U-Th)/He (ZHe) thermochronology studies, which sampled a range of basement ages and lithologies.* ***(b-e)*** *ZHe data from the Front Range presented in age vs. effective uranium concentration ([eU]) plots that reveal a systematic relationship between age and grain U-Th composition that reflects the impact of radiation damage on the retention of* ^{4}*He in zircon* (Guenthner, 2021; Guenthner et al., 2013). *The data we interpret (red and blue circles) are presented on each panel to facilitate qualitative comparison among age-[eU] trends.*

3 Low-temperature thermochronology methods in deep-time

The (U-Th)/He thermochronometers rely on the radioactive decay of U and Th, which produce stable isotopes of Pb and alpha particles (i.e., ^{4}He). Whereas the zircon U/Pb geochronometer is a routine method for determining the crystallization ages of zircon-bearing igneous rocks, He thermochronometers document rock thermal histories because, unlike radiogenic Pb, ^{4}He is only retained in minerals at relatively low temperatures on geological timescales, ~40-80˚C for the apatite He (AHe) system (Flowers et al., 2009) and ~140-220˚C for the zircon He (ZHe) system (Guenthner et al., 2013).

3.1 Radiation damage effects in U-Th/He thermochronology

The diffusive loss of He from apatite and zircon grains is controlled not only by temperature and time but also by crystallographic radiation damage produced by U and Th decay (Flowers et al., 2009; Gautheron et al., 2009; Guenthner et al., 2013; Shuster et al., 2006). Importantly, this radiation damage is itself temperature sensitive; it accumulates at low temperature and anneals at high temperature. As a result, during the thermal (i.e., time-temperature, *tT*) history of a rock, there is a co-evolution of He diffusion kinetics and radiation damage. Incorporating these effects into ZHe kinetics models (Guenthner, 2021; Guenthner et al., 2013) has transformed the ZHe system into a tool capable of resolving Precambrian thermal histories (e.g., Orme et al., 2016).

Radiation damage abundance strongly controls the temperature sensitivity of He chronometers and is a function of time and the U-Th composition of a zircon grain. For example, zircon grains of different U-Th compositions can, given a *tT* history that promotes differential accumulation and/or annealing of radiation damage, retain correspondingly different amounts of He and thus have different ZHe ages. The wider the compositional range of zircon grains is in a ZHe dataset, the greater the potential range of differential damage accumulation, and thus temperature sensitivity. The data patterns that result from this behavior (e.g., Fig. 2b-e) reflect how the abundance of radiation damage, and therefore He, in grains that share identical thermal histories varies as a function of each grain's U-Th abundance. To visualize this effect in He datasets, U-Th abundance is commonly combined into a single "effective U" concentration ($[eU]$) that is scaled by the relative alpha-particle production of U and Th ($[eU] = [U] + 0.235[Th]$) and used as a proxy for relative radiation damage abundance. The first-order shape

This article is protected by copyright. All rights reserved.

Author Manuscript

of He age-[*eU*] trends, including the age and position of inflection points and 'pediments' in ZHe datasets (e.g., Guenthner, 2021), can contain rich thermal history information, because distinctive trends can be produced by distinctive families of thermal histories. In contrast, a single He age (or, similarly, He ages from a narrow range of zircon compositions) will constrain a comparatively small part of a rock's thermal history.

In this study, we use the radiation damage accumulation and annealing models (RDAAM) for the AHe (e.g., RDAAM; Flowers et al., 2009) and ZHe (e.g., ZRDAAM; Guenthner et al., 2013) chronometers. Despite the broad efficacy of these damage-diffusivity models, their implementation of damage annealing has several known limitations. First, the part of the ZRDAAM that describes the behavior of high-damage zircon (with alpha doses of $>2.2\times10^{18}$ α/g) is based on limited empirical observations compared to other parts of the ZRDAAM (Guenthner et al., 2013). Some deep-time studies report discrepancies between ZRDAAM-predicted and observed high-[*eU*] parts of ZHe datasets (Guenthner, 2021, and references therein). Second, these damage-diffusivity models predict damage annealing using established fission-track annealing kinetics, even though alpha-recoil damage, and not fission damage, dominates the U-Th radiation damage budget of these materials. Regardless of the exact damage mechanism, the key findings of annealing studies are that radiation damage annealing (1) depends on the level of radiation damage and (2) appears to require hotter temperatures than the temperatures required completely reset the He content of a grain via diffusion (Ginster et al., 2019; Guenthner, 2021; Willett et al., 2017). As a result, the temperature sensitivity of the ZHe system, for example, can span both the temperatures required to lose He (~140-220˚C) and the hotter temperatures required to anneal radiation damage (~260-350°C for fission tracks in the current ZRDAAM). The consequences of these combined effects are magnified in rock thermal histories that span billions of years.

3.2 The Front Range proving ground for deep-time methods

Differing philosophies regarding how to use geologic context and/or statistics to narrow inverse thermal history model results are at the center of an ongoing debate about how to rigorously interpret ZHe age-[*eU*] trends in deep-time applications (Flowers et al., 2022; McDannell et al., 2022a, 2022b), and samples from Colorado's Front Range (Fig. 2) feature prominently because they meet the multiple criteria for leveraging ZHe age-[*eU*] trends.

First, ZHe datasets from the Front Range have a wide range of zircon compositions and ages (Fig. 2b-e), which have been used to investigate the behavior of He thermochronometers in Proterozoic rocks (Ault et al., 2018; Johnson et al., 2017). Second, the potential preservation of a Proterozoic thermal history is supported by $^{40}Ar/^{39}Ar$ (Ar) data that require temperatures colder than ~300 ˚C since Mesoproterozoic time (Shaw et al., 1999) and apatite fission-track data (Kelley & Chapin, 2004) that suggest most basement rocks at the surface today were near fission-track partial annealing temperatures in latest Cretaceous time, when they reached maximum net Phanerozoic burial depths prior to the onset of Laramide tectonism. Finally, key geological relationships, in particular the presence of the Neoproterozoic Tava quartzite bodies

This article is protected by copyright. All rights reserved.

Author Manuscript

(Courtney-Davies et al., 2024; Cross, 1894; Flowers et al., 2020; Siddoway et al., 2013, 2019; Siddoway & Gehrels, 2014), place the crystalline basement near Earth's surface at several times prior to the Laramide Orogeny, thus providing independent time-temperature constraints that substantially narrow the possible *tT* histories that these rocks could have experienced.

Published interpretations of ZHe data from four different parts of the Front Range (Fig. 2) have supported a broad range of Proterozoic histories, albeit with some contradictions. Inversions of ZHe data from a central Front Range sample (triangle symbols in Figs. 2, 3, and 4; Ault et al., 2018) modelled jointly with K-feldspar $^{40}Ar/^{39}Ar$ data from Longs Peak (Fig. 2a) were used to argue for rock cooling from ~200˚C to surface temperatures between ca. 1150 Ma and 500 Ma (Ricketts et al., 2021). ZHe data from Pikes Peak (Fig. 2e; Flowers et al., 2020; Havranek & Flowers, 2022) and other Front Range 'fourteeners' (Figs. 2b, d; Havranek & Flowers, 2022) have been inverted by multiple authors to resolve deep-time histories of the Front Range. One approach, similar to the one we use here, employed a Monte Carlo search of *tT* space (HeFTy; Ketcham, 2005) and enforced a Neoproterozoic surface constraint at the time of Tava sand injection, to argue for pre-Cryogenian basement exhumation to the surface by ca. 700 Ma (Flowers et al., 2020; Havranek & Flowers, 2022). In contrast, another inversion of the Pikes Peak data, which used different data handling, a Bayesian Markov-Chain Monte Carlo exploration of *tT* space (QTQt; Gallagher, 2012), and did not enforce a near-surface Tava constraint, was used to argue that these samples experienced Neoproterozoic temperatures of ~200˚C at ca. 700-660 Ma, followed by cooling to surface conditions by ca. 600 Ma (McDannell et al., 2022b)—a history that is inconsistent with the near-surface formation of the Tava injectites and the pre-Cryogenian exhumation hypothesized by Flowers et al. (2020).

Previous work by the author team includes a published AHe and ZHe data repository item from the central Front Range (Murray, Niemi, et al., 2022; Fig. 2) and a methods paper on thermal history modeling approaches that included deep-time inversions of three samples from the aforementioned data repository (Murray, Stevens Goddard, et al., 2022). Here, we use a two-stage approach to deep-time thermal history analysis (Murray, Stevens Goddard, et al., 2022), which inverts ZHe and AHe data while quantitatively honoring $^{40}Ar/^{39}Ar$ data, constraints from the geologic record, and the temperatures necessary to anneal radiation damage in zircon. We present sensitivity tests of new and published inversions, which corroborate the capacity of Ar data to provide critical Proterozoic thermal constraints on the exploration of temperatures necessary to anneal radiation damage in zircon grains and thereby account for radiation-damage effects in ZHe data (Murray, Stevens Goddard, et al., 2022). We also adopt the methodology outlined in Murray, Stevens Goddard et al. (2022) to interpret other He data from our central Front Range dataset (Murray, Niemi, et al., 2022). Finally, supported by new zircon U/Pb data on the emplacement of six Colorado Mineral Belt stocks, we interpret these thermal history modeling results in their full geologic and thermochronologic context.

4 Sampling and analytical procedures

This article is protected by copyright. All rights reserved.

Author Manuscript

The samples of Paleoproterozoic and Cretaceous-Paleogene crystalline rocks used in this study were collected for U/Pb (this study) and (U-Th)/He (Murray, Niemi, et al., 2022) analysis from the Front Range west of Boulder, Colorado (Figs. 2a, 3, Table 1). Zircon U/Pb (n=6) and apatite He (n=2) analyses were performed on samples collected from six CMB stocks (Table S1; Fig. 3) to determine the timing of potential thermal perturbation resulting from CMB magmatism. Apatite and zircon He analyses were performed on samples of Paleoproterozoic basement rocks collected in two short vertical profiles, one near Boulder Canyon (referred to here as the range front samples; 1905–2469 m, n=7) and the other ~30 km west of the range front, near the Continental Divide (referred to here as the divide samples; 3254–3925 m, n=4).

Samples were processed using standard rock crushing followed by density and magnetic mineral separation techniques. Zircon U/Pb analyses were conducted by laser ablation multicollector inductively coupled plasma mass spectrometry at the Arizona Laserchron Center (Text S1), following the methods of Gehrels et al. (2008). Zircon $^{238}U/^{206}Pb$ ages of the CMB stocks are reported with 2σ uncertainties. See Murray, Niemi, et al. (2022) for (U-Th)/He analytical procedures. AHe and ZHe ages are reported as a mean and standard deviation for samples with ≤15% age variability or as an age range for samples with >15% age variability.

5 Geochronologic and thermochronologic results

Latest Cretaceous and early Cenozoic U/Pb and He ages are abundant in the central Front Range dataset (Fig. 4; Table 1) and reflect the most recent period of crystalline rock formation and cooling, whereas 11 single-grain ZHe ages older than 85 Ma suggest preservation of pre-Cretaceous thermal information exclusively in samples from the range front. AHe and ZHe ages from the divide vertical profile vary systematically with sample elevation but are uniformly latest Cretaceous and younger. In contrast, samples from the range front yielded zircon grains with a large spread of He ages (50-607 Ma) and [*eU*] compositions (289-2344 ppm) that form an age-[*eU*] pattern characteristic of radiation damage effects.

Ages from the CMB stocks refine previously published crystallization and cooling ages compiled by Wilson and Bryant (2006) and suggest that there were two brief pulses of CMB magmatic activity in the central Front Range in latest Cretaceous (ca. 67 Ma) and Eocene (ca. 47 Ma) time (Figs. 3, S3; Tables S1, S2). Zircon U/Pb ages from the Eldora (i.e., Bryan Mountain), Caribou, and North Fork stocks near the Continental Divide are 67.2±0.87, 66.6±0.79, and 66.3±0.75 Ma, respectively. In contrast, the Sunset, Sugarloaf, and Bald Mountain stocks from the middle of our study area are 47.2±0.48, 46.6±0.52, and 47.4±0.57 Ma. AHe ages from the Sunset and Sugarloaf stocks are 48±7.3 and 55±8.1 Ma, respectively (Table 1, Figs. S4, S5). These average cooling ages are within error of the crystallization ages and thus support rapid post-emplacement cooling to <60 ˚C at ca. 47 Ma. However, there are single-grain AHe ages that are older than stock emplacement (Fig. S5). This suggests that some chemical complexity (e.g., Murray et al., 2014; Spiegel et al., 2009), perhaps related to CMB mineralization, has impacted the AHe system in the CMB rocks. Therefore, we do not use AHe data from the CMB stocks for quantitative thermal history analysis.

This article is protected by copyright. All rights reserved.

Author Manuscript

AHe ages from the Paleoproterozoic crystalline rocks are Paleocene-Eocene and have no significant intra-sample age variability as a function of [*eU*] or grain size (Table 1, Figs. S4, S5). The seven range front samples have a combined mean AHe age of 57±2 Ma. At the divide, ages vary with sample elevation (Fig. S4a); average AHe ages range from 55±2.0 Ma to 46±2.4 Ma from the highest elevation to lowest elevation samples, respectively. The youngest AHe ages correspond to the latest phase of CMB activity documented by the zircon U/Pb data.

Most Paleoproterozoic crystalline rock samples yield ZHe ages with significant (>15%) single-grain age variability (Table 1; Figs. 2c, 4, S4) that corresponds with grain [*eU*] (Fig. 4). In the divide samples, single-grain ZHe ages from the highest elevation sample are 73–108 Ma, and the two lower samples have mean ages of 75±7 and 72±6 Ma ([*eU*] = 289-921 ppm). At the range front, single-grain ZHe ages are 50–607 Ma ([*eU*] = 379-2344 ppm). Negative-slope ZHe age-[*eU*] trends (Figs. 2b-e, 4) are consistent with radiation damage effects in zircon (Guenthner et al., 2013). The youngest ZHe ages from both parts of our study area overlap in time with the CMB plutonism documented by the zircon U/Pb data (Fig. 4). Six high-[*eU*] zircon grains (>1200 ppm) from the range front samples have reproducible ages that form a >1000 ppm wide 'age pediment' (e.g., Guenthner, 2021) with a mean age of 61 ± 7.5 Ma. The single-grain ZHe ages older than 85 Ma (n=11) and the high-[*eU*] grains that retain He suggest that this age-[*eU*] trend preserves a pre-Cretaceous thermal history.

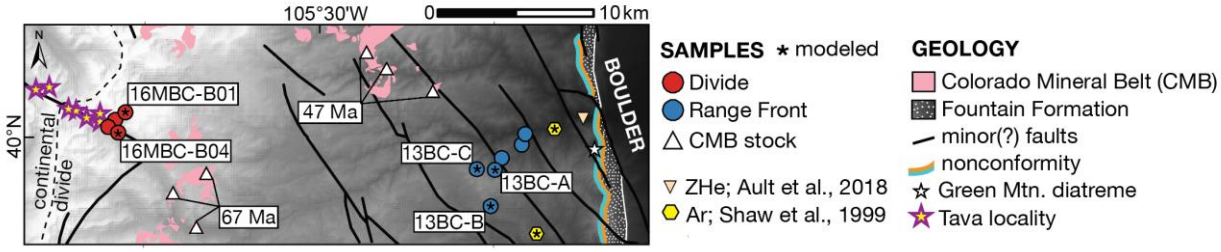


Figure 3*. Digital elevation model of the study area with sample locations and key geologic features. Location of faults and the Fountain Formation modified from Tweto* (1979)*. Tava localities and Colorado Mineral Belt stocks from the Estes Park* (Cole & Braddock, 2009) *and Denver West* (Kellogg et al., 2008) *geologic map sheets. CMB emplacement ages are from this study. The Fountain Formation and younger Mesozoic stratigraphy, along with the nonconformity between them and the basement rocks, dip steeply to the east as the result of shortening, rock uplift, and exhumation during the Laramide orogeny.*

This article is protected by copyright. All rights reserved.

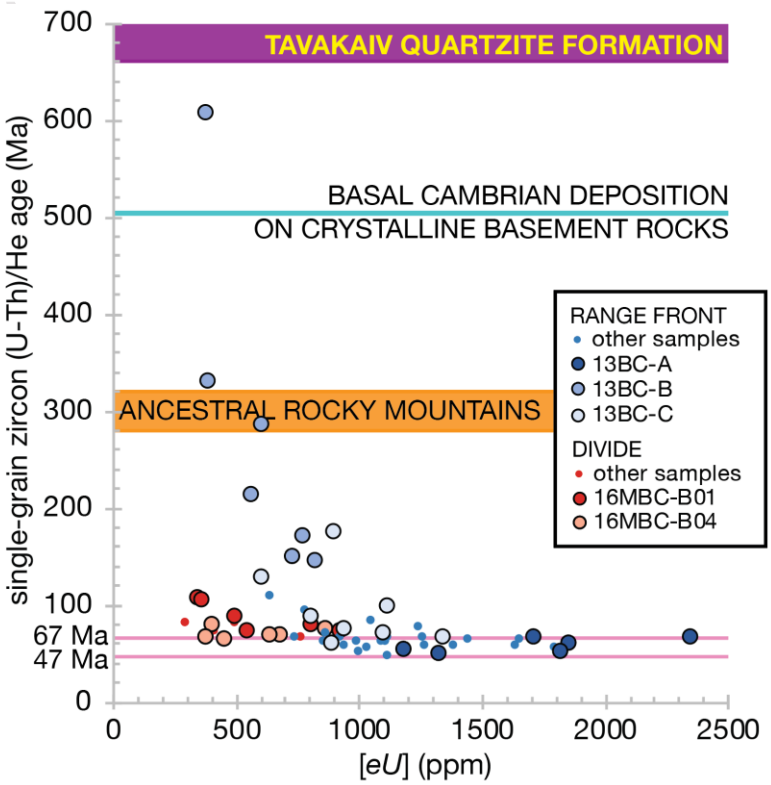


Figure 4. *Single-grain ZHe ages from the central Front Range* (Murray, Niemi, et al., 2022) *plotted against [eU]. Large symbols identify data used for thermal history modeling by Murray, Stevens Goddard et al. (range front samples) and in this study (divide and range front samples). Overlays (colors key to Fig. 3) indicate the known major geologic events or features in the Front Range that place samples <2 km from Earth's surface. The zircon U/Pb ages of six Colorado Mineral Belt stocks are represented by pink lines at 67 Ma and 47 Ma and illustrate how this plutonism overlaps in time with the youngest ZHe ages.*

6 Thermal history modeling

In order to identify the range of thermal histories consistent with both the geologic record and available AHe, ZHe, biotite $^{40}Ar/^{39}Ar$ (Ar), and hornblende Ar data from the central Front Range, thermal history modeling was performed using the program HeFTy v.1.9.3 (Ketcham, 2005). Here, we include the range front inversion results from Murray, Stevens Goddard, et al., (2022) (e.g., Fig. 5a) with new sensitivity analysis and new inversion results (Fig. 5b, c) for divide samples using the same methodology as Murray, Stevens Goddard, et al. (2022). Additional details regarding the model design and data input decisions can be found in Supplementary Text S2.

6.1 Modeling principles, data inputs, and design

We selected HeFTy for this study because it uses a simple, non-converging Monte Carlo approach to explore *tT* space and an inversion scheme that can accommodate many degrees of freedom. It is therefore well suited to identifying the range of thermal histories that are consistent

This article is protected by copyright. All rights reserved.

Author Manuscript

with the data, while leveraging the power of the extant geologic record and exploring a wide range of possible solutions during periods when little independent geologic information is available. In the statistical philosophy that underpins HeFTy, the simplest answer is not necessarily the best one. With intentional use of exploration and constraint boxes in *tT* space, the user guides the HeFTy inversion algorithm to map out complexity in parts of *tT* space that are of interest (e.g., exploring Neoproterozoic time) while strictly honoring specific parts of the geologic record relevant to the thermal history (e.g., constraining paths to being cold and at Earth's surface for sediment deposition on a known unconformity surface). Additionally, with HeFTy the user can systematically explore and analyze the sensitivity of inversion results to various aspects of the model design and data inputs (Murray, Stevens Goddard, et al., 2022).

6.1.1 U-Th/He data inputs

Because HeFTy limits the degrees of freedom permitted in tT space, there is a corresponding limit to the number of data inputs (Ketcham, 2005). Therefore, it is necessary to discretize continuous He age-[*eU*] trends as representative data inputs that capture the first-order trend rather than using the complete set of individual grains directly (Fig. S6; Text S2). This approach is appropriate for datasets with continuous, monotonic age-[*eU*] trends, such as the datasets used here. Further, sensitivity tests of data input decisions provide a means to assess how these decisions contribute to the inversion results (Murray, Stevens Goddard, et al., 2022).

To create He data inputs, measured ZHe and AHe ages were grouped by [*eU*] in order to create synthetic grains with representative He age, [*U*], [*Th*], and grain size (Fig. S6; Text S2). ZHe data were grouped in order to capture up to four first-order features of each age-[*eU*] trend that provide thermal history information that the current ZRDAAM can resolve (e.g., Guenthner, 2021): the lowest [*eU*] ages, the highest [*eU*] ages, the position of inflection point(s) in the age-[*eU*] pattern, and the presence and extent of age pediments.

In this study, we individually inverted He data from the highest (16MBC-B01) and lowest (16MBC-B04) elevation divide samples because they have different ZHe and AHe ages that vary systematically with elevation (Figs. 4, S4a, S5b, S6). We also provide the previously published (Murray, Stevens Goddard, et al., 2022) and new sensitivity tests produced using He data from three range front samples (13BC-A, 13BC-B, 13BC-C, Figs. 3, 4) that span the entire range front ZHe age-[*eU*] trend. These three samples were combined and modeled as a single sample '13BC-ABC' (Fig. S6a) in order to find the *tT* histories that can produce the entire range front ZHe age-[*eU*] pattern. These three samples were collected within ~200 m elevation and 2.5 km spatially (Fig. 3) and have a mean AHe age of 58±4.3 Ma, supporting the assumption that these samples share a common *tT* history, and thus can be modeled as a single sample.

6.1.2 Ar data inputs

Ar data inputs were created from published Mesoproterozoic hornblende (R30416-2, average 1449 ± 7 Ma) and biotite (R30416-2 and R30416-3, average 1351 ± 22 Ma) $^{40}Ar/^{39}Ar$ ages (Shaw et al., 1999) from the range front near our samples (Murray, Stevens Goddard, et al.,

This article is protected by copyright. All rights reserved.

Author Manuscript

2022). Although HeFTy is not pre-loaded with kinetics models for the diffusion of Ar in hornblende or biotite, the program can model any diffusion-based chronometric system if the user manually inputs published kinetics parameters and a grain size. In the case of an inverse model, a measured age and error must also be provided. For the biotite Ar system, we used the frequency factor (D_0) and activation energy (E_a) values for the Cooma biotite reported in McDougall and Harrison (1999; their Figure 5-14)). The Cooma biotite has a similar composition (Ann_{56}) as the biotite grains from the Shaw et al. (1999) samples ($Ann_{43\text{-}59}$). For the hornblende Ar system, we used the D_0 and E_a values from Harrison (1981) as reported in McDougall and Harrison (1999; their Figure 5-17).

A two-stage approach that quantitatively incorporates published hornblende and biotite Ar ages was employed in the inversions (Murray, Stevens Goddard, et al., 2022). First, just the Ar data were modeled to produce "Ar-only" inversion results, using broad *tT* boxes designed to explore a wide range of monotonic and non-monotonic histories with no geologic constraints. Parallel "He-only" inversion results, produced using just the He data and the same broad *tT* boxes, were overlaid on the Ar-only results in *tT* space to provide a baseline assessment of the independent resolving power of these two datasets. Then, the results of the Ar-only inversion were used to define the high-temperature bounds of the exploration and constraint boxes used in the inversions of the He data that we use for geological interpretations. Reported biotite and hornblende Ar ages are consistent across the Front Range region (Shaw et al., 1999), so the same thermal history bounds derived from the Ar-only models are used as constraints for inversions of the range front and divide samples. This two-stage approach permits us to model Ar ages with published kinetics while leveraging the overlapping temperature sensitivities of radiation damage annealing in the ZHe system according to the ZRDAAM radiation damage annealing model (~260-350˚C; Guenthner et al., 2013) and Ar retention in biotite (~250-400˚C; McDougall & Harrison, 1999).

6.1.3 Model design

The inversions in this study were designed to explore *tT* space in the following ways. All inversions start at 1750-1700 Ma and 800-750˚C at the time of the crystallization of the Boulder Creek batholith (Premo & Fanning, 2000) and end at the modern mean annual temperature at the sample location. In addition to these starting and ending conditions, for each inversion various combinations of *tT* boxes were used, depending on the intention of a particular inversion run (e.g., using all available information and data, Fig. 5; or testing the sensitivity of a result to a particular design choice, Figs. 6, 7). The inversions that we use for geologic interpretations combine all available information and thus have identical *tT* boxes that (1) require Mesoproterozoic cooling to fit the Ar data; (2) explore a wide range of thermal histories that get no hotter than 250-285 ˚C between ca. 1300 Ma and 650 Ma and again between 650 Ma to 500 Ma; (3) implement a "Tava constraint" by requiring samples to be at T <60˚C at 700-650 Ma, 540-500 Ma, and 320-280 Ma; and (4) honor the timing and magnitude of burial during Phanerozoic time prior to the Laramide orogeny. Two side-by-side constraint boxes between

This article is protected by copyright. All rights reserved.

Author Manuscript

1475 and 700 Ma permit non-monotonic histories during this time when there is no independent geologic information. See Supplementary Text S2 for additional description of this and all other *tT* constraints. For all inversions, HeFTy was run for the number of *tT* paths necessary to find 100 good-fit paths or 1,000,000 attempted paths.

HeFTy inversion results—which are visualized in *tT* space as individual *tT* paths that fit the data according to "good" or "acceptable" fitness criteria (Ketcham, 2005; Ketcham et al., 2009)—can *require*, be *consistent with*, or *exclude* specific thermal histories (Flowers et al., 2015). For example, it is common for constraint boxes that actively narrow the range of possible solutions (e.g., to enforce an observation from the rock record) to be uniformly filled with good- and acceptable-fit paths. In this case, the data being modeled would be *consistent with* that *tT* constraint, but they may not require it. In contrast, if only part of a *tT* box is filled by good and acceptable-fit paths, then a subset of specific temperature conditions during that interval of time are *required* to fit the data; however, because thermal histories are time-integrative, this requirement also depends on user assumptions (Ketcham, 2005, 2024) and how they are implemented as the other data handling and model design choices.

6.2 Ar-only and He-only thermal history results

The Ar-only inversion result with no geologic constraints places high-temperature bounds on the Neoproterozoic-Recent thermal history of basement rocks in the central Front Range (Fig. 6a, yellow field; Murray, Stevens Goddard, et al., 2022). The hornblende Ar data narrowly constrain the timing of cooling below ~450˚C to between 1500 Ma and 1400 Ma, consistent with the interpretations of Shaw et al. (1999). Additionally, the Ar-only model results demonstrate that in order to preserve the observed ca. 1350 Ma biotite Ar ages, the rocks must have been colder than ~250 ˚C on long (>~100-Myr) timescales and colder than ~285 ˚C on relatively short (<~100-Myr) timescales after ca. 1275 Ma. This information is used to define three Proterozoic *tT* constraint boxes and the <1275 Ma high-T bound in the combined inversion models. The parallel He-only inversion result (Fig. 6a, grey fields) illustrates that the He data alone are consistent with temperatures as hot as 450˚C for the entirety of Proterozoic time, suggesting that the Ar plays a key role in narrowing the range of permissible *tT* histories (Murray, Stevens Goddard, et al., 2022).

6.3 Combined thermal history results

The thermal history inversion results that fit the AHe and ZHe data, use *tT* constraints derived from Ar-only *tT* inversions, and honor all available geologic constraints for the Front Range region are presented in Figure 5 for both the range front and the divide sample sets. The range front inversion result reveals a long-lived late Neoproterozoic thermal event (Fig. 5a; Murray, Stevens Goddard, et al., 2022). After Tava injection ca. 700-650 Ma, rocks at the range front were heated to a late Neoproterozoic peak temperature (T_p) of 240-285 °C prior to cooling to T < 60°C by ca. 500 Ma. During this heating event, the *tT* paths were hotter than 220°C for at least 18 Myr and, on average, for 76±29 Myr (Fig. S7a). A single acceptable-fit *tT* path (Fig. 5a,

This article is protected by copyright. All rights reserved.

Author Manuscript

blue) does not require post-Tava heating. However, it resides at T > 240 ˚C from ca. 1400 to 700 Ma; a forward model of this *tT* history predicts a 1075 Ma biotite Ar age, which is not consistent with the Ar data.

The two divide sample inversion results, from the lowest and highest elevation parts of the divide transect, have differences in their the Late Cretaceous T_p that is consistent with their ~750 m vertical separation, with mean good-fit T_p of ~190°C and >200°C, respectively (Figs. 5b,c). In contrast, the range front result requires a narrower, colder Late Cretaceous mean good-fit T_p of ~170°C (Fig. 5a). A post-Tava Neoproterozoic heating and cooling signal is not present in the divide inversion results (Figs. 5b, c). Instead, the divide inversion results are consistent with a wide range of post-Tava thermal histories.

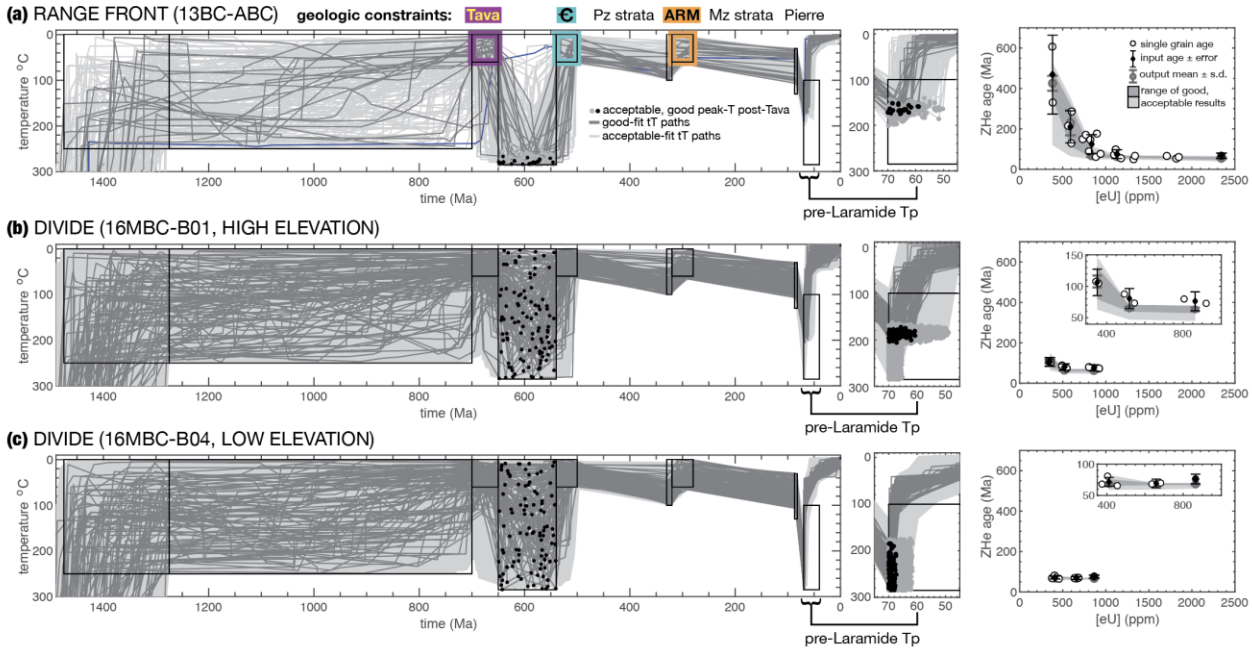


Figure 5. *Combined thermal history modeling results; see Fig. 3 for spatial location of geologic constraints highlighted in color. Black boxes define the parts of time-temperature (tT) space explored during each inversion; they are identical in these three inversions. The left panel presents the good- and acceptable tT paths. The right panel presents the corresponding fit to the ZHe age-[eU] trend.* ***(a)*** *The inversion result for the range front age-[eU] trend represented by samples 13BC-A, 13BC-B, and 13BC-C (Fig. 4), from Murray, Stevens Goddard, et al. (2022, their figure 6a). All good-fit and all but one acceptable-fit paths have late Neoproterozoic reheating with peak temperatures (T_P) of 240-285 ˚C. The outlier acceptable-fit path (blue) is too hot for too long prior to Tava emplacement to be consistent with Mesoproterozoic biotite $^{40}Ar/^{39}Ar$ ages, which helps demonstrate the principal reasons Neoproterozoic heating is required (Murray, Stevens Goddard et al., 2022). Latest Cretaceous (i.e., pre-Laramide) peak temperatures (T_P) are also tightly constrained by this result (middle panel).* ***(b,c)*** *The inversion results for divide samples (Fig. 4), which do not resolve a particular Proterozoic history but do provide constraints on the pre-Laramide peak temperatures that are consistent with their relative elevations.*

This article is protected by copyright. All rights reserved.

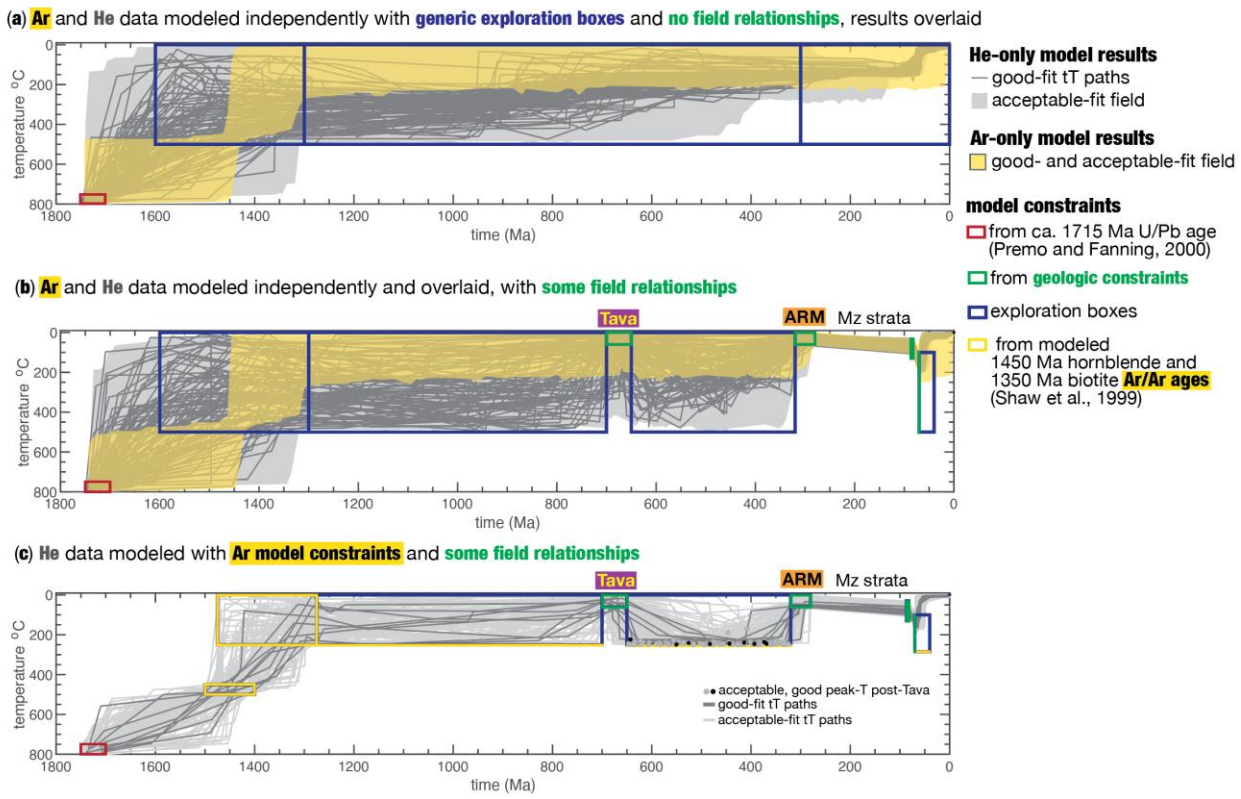


Figure 6*. **(a)** Ar-only (yellow) and He-only (grey) thermal history inversions of the range front samples are overlaid to demonstrate how the Ar and He data independently constraint the range front thermal history (Murray, Stevens Goddard, et al., 2022). The Ar data require cold temperatures from ca. 1300 Ma to present but are otherwise insensitive to details of the Neoproterozoic-Recent history. Similarly, the He data alone do not require a particular Proterozoic history; they do, however, constrain the most recent (Laramide-age) cooling event that these rocks experienced. **(b)** Adding geologic constraints (green boxes) to the Ar-only and He-only model designs does not change the Proterozoic tT results. **(c)** A variation on the range front inversion (Fig. 5a) illustrates the Murray, Stevens Goddard, et al. (2022) method for translating the Ar-only results into the exploration tT bounds (yellow) that were used in the combined inversions.*

6.4 Sensitivity testing and implications for deep-time thermochronology

Model design and data handling choices affect the features of the Neoproterozoic thermal event in the combined thermal history results, and thus sensitivity analyses are required to understand how each of these decisions is related to an inversion outcome (Murray, Stevens Goddard, et al., 2022). Previously, it was found that the Neoproterozoic heating and cooling in the range front inversion result (Fig. 5a) is a consequence of three factors: the Ar ages requiring temperatures <250-285˚C since Mesozoic time (e.g., Fig. 6), the extant geologic record placing the samples in the near surface before ca. 650 Ma and during most of Phanerozoic time, and the dated zircon grains having <700 Myr of net radiation damage accumulated in their crystallographic structure. In this study, we build on these published insights with new sensitivity

This article is protected by copyright. All rights reserved.

analyses, which are fundamental to making a robust geological interpretation. Specifically, we explore how the near-surface geological constraints and the high-[*eU*] zircon data control the resolution of the timing and magnitude of the Neoproterozoic heating event and subsequent cooling.

6.4.1 The role of geologic constraints

Systematically changing which near-surface geological constraints are implemented in *tT* space demonstrates that the timing, but not the magnitude, of heating and cooling in pre-Mesozoic time is strongly controlled by these model design choices. For example, if heating to T = 250-285˚C is permitted after the ARM near-surface constraint, then heating to such temperatures in Neoproterozoic time is not required (Fig. S9); however, the Mesozoic stratigraphic record in the Denver basin precludes such histories. Additionally, in our inversion design (Fig. 5) all *tT* paths were required to be <60˚C at three times prior to Late Cretaceous time: 700-650 Ma, for Tava emplacement; 540-500 Ma, for Cambrian deposition on crystalline basement; and 320-280 Ma for Fountain Formation deposition on crystalline basement. Alternative interpretations of these geologic features yield some differences in the timing and duration of heating and cooling. For example, permitting a longer age range for Tava formation (Fig. 7a; Siddoway & Gehrels, 2014) correspondingly expands the potential timing of Neoproterozoic heating (Fig 7a). The possible age and duration of heating is further expanded if the surface constraint in Cambrian time is relaxed (Fig. 7b) or if both the Tava and Cambrian constraints are relaxed (Fig. 7c). Each alternative still requires heating for tens of millions of years at temperatures sufficient to reset both the He and radiation damage content of zircon grains during Neoproterozoic-Paleozoic time (Fig. S7), however, the timing of the peak temperature conditions and subsequent cooling to near-surface conditions depends on the geologic constraints, not the thermochronologic data (Murray, Stevens Goddard, et al., 2022).

This article is protected by copyright. All rights reserved.

Author Manuscript

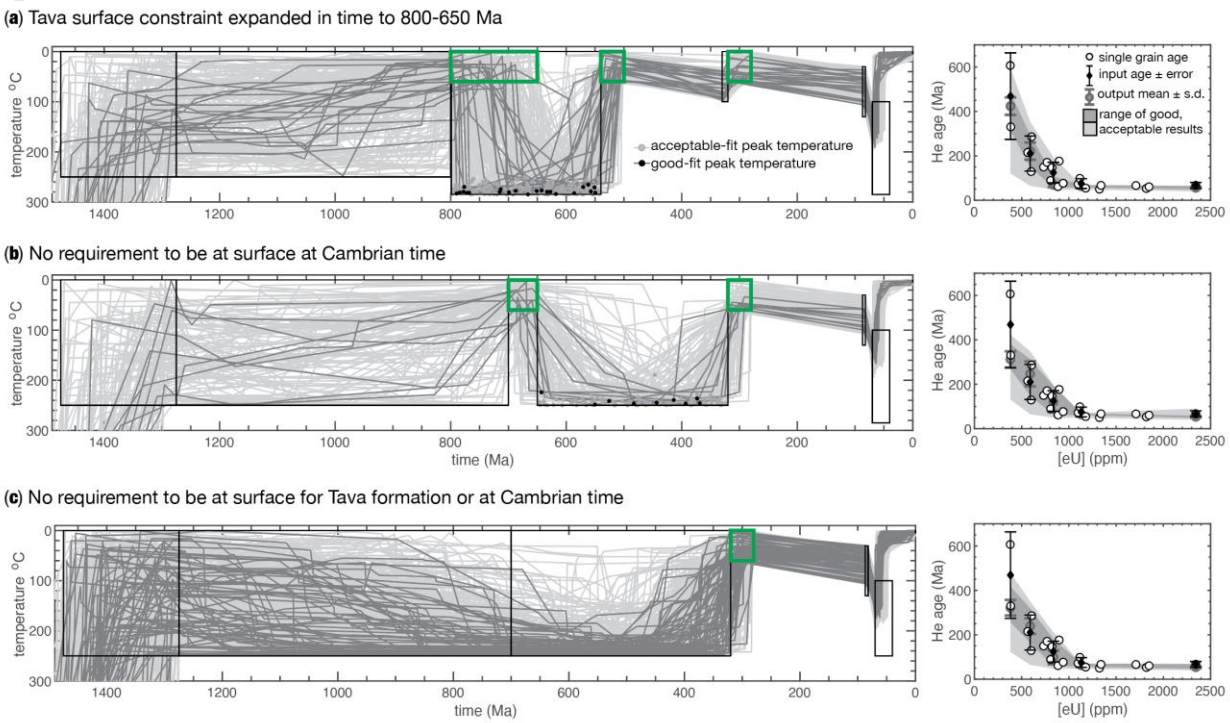


Figure 7. *Inverse sensitivity tests using alternative translations of geologic observations into tT space (green tT boxes; Murray, Stevens Goddard, et al., 2022, their figure 7). In each case, all good- and acceptable-fit paths are hot in Neoproterozoic-Paleozoic time but the timing of this heating, and the subsequent cooling, depends on the near-surface constraints.* ***(a)*** *Expanded Tava age constraint.* ***(b)*** *No requirement to be at the surface in Cambrian time. This result is also presented in Fig. 6c, but here we zoom into Mesoproterozoic-Recent time and T<300 ˚C.* ***(c)*** *No Proterozoic or Cambrian near-surface constraints.*

6.4.2 The role of the high-[eU] zircon grains

Among all the model design and data handling choices, the highest-[*eU*] zircon data input appears to most strongly control the requirement of Neoproterozoic heating (Murray, Stevens Goddard, et al., 2022). Here we explore two alternative scenarios where (1) the single highest-[*eU*] grain (2344 ppm) is excluded (Fig. 8a; new to this study) or (2) all the high [*eU*] grains (>1200 ppm) are excluded (Fig. 8b, from Murray, Stevens Goddard, et al., 2022). In the first scenario, excluding the highest-[*eU*] grain does not significantly alter the inversion results shown in Figure 5a. The average post-Tava T_P is 233 ± 64˚C (all paths), with 96% of good-fit paths and 89% of acceptable fit paths requiring post-Tava T_P > 140˚C, into the ZHe partial-retention zone. Furthermore, the four good-fit paths that do not heat to T_P >140˚C after Tava emplacement are all at T_P > 200˚C for more than 190 Myr prior to Tava emplacement (Fig. 8a); these *tT* histories predict biotite Ar ages that are 80-143 Ma younger than the observed mean age (1351 Ma). In the second scenario, all the high-[*eU*] zircon data are removed, which truncates the age-[*eU*] trend at ~1200 ppm [*eU*]; still, 94% of good-fit paths and 75% of acceptable-fit paths require post-Tava heating to T_P > 140 ˚C (Figs. 8b, S8a). In other words, even excluding the six highest-[*eU*] grains

This article is protected by copyright. All rights reserved.

that form the 61 ± 7.5 Ma age pediment, the inversion result is consistent with, but less strongly supports, significant post-Tava heating.

Forward modeling further illustrates the contribution of the biotite Ar ages to narrowing the *tT* histories required by high-[*eU*] grains (Fig. 8c): if a zircon grain of >2300 ppm [*eU*] is cold enough to accumulate radiation damage for more than ~700 Myr, then the current ZRDAAM predicts that it becomes so damaged that it cannot retain He and will have a 0 Ma age. Therefore, the 67 Ma ZHe age measured in a zircon grain with 2344 ppm [*eU*], and the age pediment it contributes to defining, place a constraint on the maximum duration of time these rocks could have been cold enough to accumulate radiation damage since Paleoproterozoic time. As Murray, Stevens Goddard, et al. pointed out, the outlier *tT* path in the preferred result (Fig. 5a, blue path) is also a manifestation of this limit on the net radiation damage. The outlier path does not have post-Tava heating because it is at T >240˚C until cooling to near-surface conditions after 700 Ma, and therefore it does not accumulate Proterozoic radiation damage that needs to be reset after Tava formation. Thus, as demonstrated by Murray, Stevens Goddard, et al. (2022), the narrow range of post-Tava peak temperatures required in the range front inversion result reflect the maximum cumulative radiation damage permissible in the highest-[*eU*] zircon grain, combined with the maximum temperature constraints provided by the biotite Ar data.

Our forward modeling also demonstrates the contribution of the old, low-[*eU*] ZHe ages. If a sample is heated to >200˚C in latest Cretaceous time, then the ZRDAAM can fit, for example, the three ZHe ages from grains with [*eU*] of 1700-1850 ppm (i.e., the high-[*eU*] input in Fig. 8a). However, this hot pre-Laramide T_P would also reset the He content of the low-[*eU*] grains (Fig. 8c, orange lines). Thus, the old high-[*eU*] ZHe ages place a constraint on the recent peak temperatures our samples experienced. This is also clear in the differences between the divide and range front age-[*eU*] trends and inversion results (Fig. 5).

This article is protected by copyright. All rights reserved.

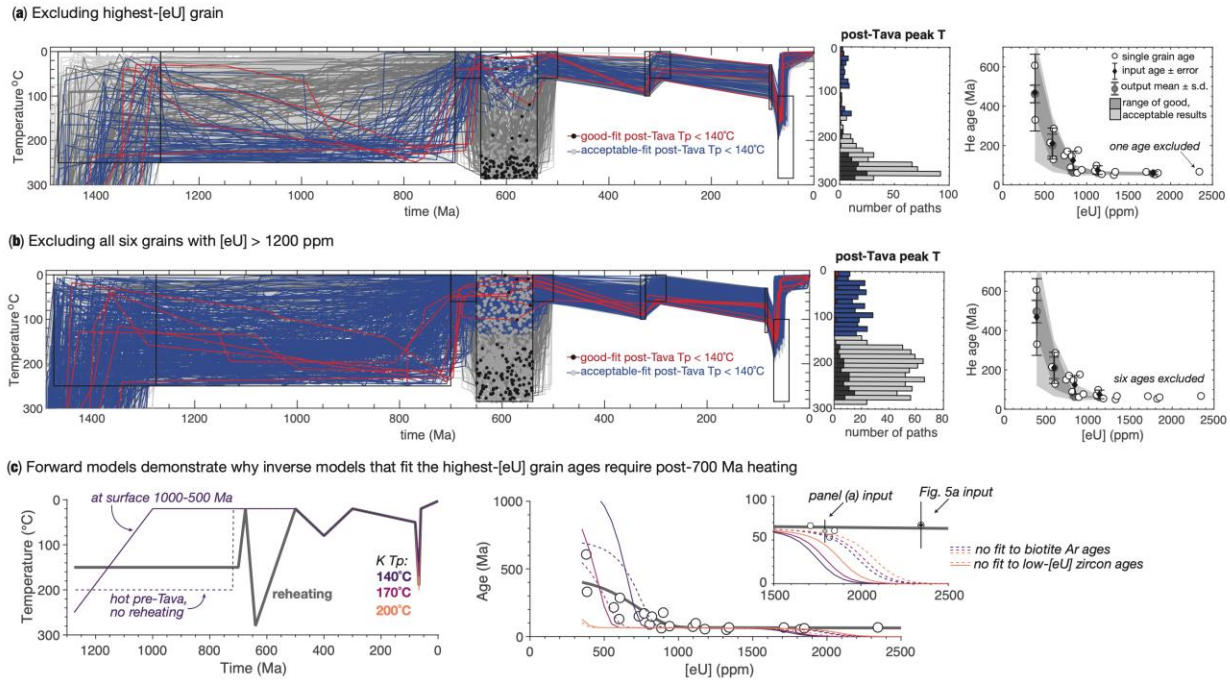


Figure 8. *Inverse and forward models demonstrate the role of the youngest, highest-[eU] zircon grains in documenting a Neoproterozoic heating signal. (**a**) Scenario 1 excludes the highest-[eU] age from the data inputs. (**b**) Scenario 2 excludes the six high-[eU] grains that form the 61 ± 7.5 Ma age pediment and truncates the age-[eU] trend at 1130 ppm (Murray, Goddard, et al. (2022; their figure 6b). (**c**) Forward models, produced using the code of Guenthner (2021), further demonstrate how the young, high-[eU] part of a ZHe age-[eU] trend can document details of a sample's Proterozoic thermal history. The thick dark grey line is a 'reheating' history like the family of paths resolved by the range front inversion result (Fig. 5a), whereas the thinner lines represent other end-member Proterozoic histories that do not honor the biotite Ar data (dotted lines) or fit the highest-[eU] zircon grain ages (solid lines). The impact of varying the latest Cretaceous T_P on the ZHe age-[eU] trend is illustrated with variable colors.*

6.5 Discussion of the thermal history results

Notable features in the combined inversion results (Fig. 5), which honor all available geologic constraints and thermochronologic data, include a narrow range of Late Cretaceous (i.e., pre-Laramide Orogeny) peak temperatures (T_p) and a distinctive late Neoproterozoic thermal event. The Neoproterozoic heating is documented by the range front samples but not by the divide samples. This difference between the divide and rage front results is not surprising, because the ZHe ages from the divide samples are much younger (<125 Ma) and from a narrower range of zircon compositions (~300-900 ppm [*eU*]) than the range front samples (~400-2400 ppm [*eU*], Fig. 4), thus suggesting that the range front samples are sensitive to variations in Proterozoic thermal histories due to their wide range of zircon [*eU*]. Furthermore, the inversion results suggest that the divide samples do not document a specific Neoproterozoic thermal history because they experienced warmer Late Cretaceous T_p than samples at the range front.

This article is protected by copyright. All rights reserved.

Author Manuscript

These warmer Cretaceous peak temperatures, likely a result of heating during CMB pluton emplacement and/or spatially variable Cretaceous burial (Kelley & Chapin, 2004), were sufficient to reset the He content of the low-[*eU*] zircon grains in these samples and thereby overprint any signal of the pre-Laramide thermal history. The range of Late Cretaceous T_p documented in each inversion (Fig. 5) is consistent with those reported in previous studies (Ault et al., 2018; Johnson et al., 2017; Kelley & Chapin, 2004) (Havranek and Flowers, 2022).

The sensitivity analysis we present (Fig. 8) demonstrates that the narrow range of Neoproterozoic T_p (240-285°C) in the range front inversion result (Fig. 5a) is bounded at low temperature by the ZHe data, in particular the 61 ± 7.5 Ma age pediment. We note that the inclusion of high-[*eU*] grains in our thermal history analysis is a departure from previous Front Range and some other deep-time studies. Discrepancies have been reported between the observed ages of high-[*eU*] grains and the very young or 0 Ma ages predicted for those grains by the ZRDAAM (Johnson et al., 2017; Mackintosh et al., 2019; Orme et al., 2016), which has been linked to the limited ability of the current ZRDAAM to predict the behavior of highly-damaged zircons (Guenthner, 2021, and references therein). These discrepancies have prompted some front range studies to exclude the highest-[*eU*] parts of age-[*eU*] trends from their thermal history analysis (e.g., Havranek & Flowers, 2022). However, mismatches between observed and predicted cooling ages can arise from at least two possible causes (Johnson et al., 2017): (1) the kinetics of the ZRDAAM are incomplete or (2) the thermal history model designs are flawed. Our analysis demonstrates that designing inversions that explore temperatures capable of resetting Proterozoic radiation damage (>250˚C) is one way to fit high-[*eU*] ZHe ages with the current ZRDAAM model. Moreover, our results suggest that arbitrarily limiting the *tT* space explored by inversions to temperatures below those required to anneal radiation damage in the ZHe system (<~220˚C) or truncating the high-[*eU*] parts of age-[*eU*] trends may significantly limit the ability to resolve Proterozoic thermal histories with ZHe datasets.

Although there are some circumstances in which it may be appropriate to exclude high-[*eU*] ZHe ages from a quantitative thermal history analysis due to concerns about using the current ZRDAAM to fit ages from highly damaged zircon grains, the thermochronologic data from the central Front Range do not have any hallmarks of high-damage zircons, such as "inverted" ZHe ages that are younger than AHe ages or apatite fission-track ages. Instead, the range front ZHe ages form a 61 ± 7.5 Ma pediment that clearly corresponds to the most recent (Laramide-age) period of substantial rock cooling in the Front Range region. This cooling is independently documented by (1) the apatite He data from the central Front Range used in this study (Table 1, Figs. S4, S5; Murray, Niemi, et al., 2022); (2) the zircon U/Pb crystallization ages from the CMB plutons, which bracket the ZHe age pediment (Fig. 4); (3) apatite fission-track data from the central Front Range (Fig. S4; Kelley & Chapin, 2004) and (4) apatite fission-track data and stratigraphic evidence in the Denver Basin (Kelley, 2002).

The sensitivity analysis we present (Fig. 8) also emphasizes that the narrow range of Neoproterozoic T_p (240-285°C) in the range front inversion result (Fig. 5a) is bounded at high

This article is protected by copyright. All rights reserved.

Author Manuscript

temperature by the Ar data (Murray, Stevens Goddard et al., 2022). This is because the open-system behavior of the biotite Ar system, as defined by the Cooma biotite Ar kinetics, occurs at temperatures ~≥250˚C on very long (10^2-10^3 Myr) timescales—such as the ~700 Myr period prior to Tava emplacement. This temperature sensitivity agrees with previous calculations of partial-retention temperatures for Ar chronometers (Reiners & Brandon, 2006), which estimate that for hold times of >100 Myr, the biotite Ar system remains partially open (retaining 90% of Ar) at temperatures as low as 225-200˚C.

Future advances in the understanding of radiation damage annealing in zircon and the ability to jointly model He and Ar data may shift the exact range of Neoproterozoic temperatures supported by the He and Ar data used in this study. However, the primary result of the range front model—that the ZHe system was completely reset (both He and radiation damage) in late Neoproterozoic time, but the biotite Ar system was not—is robust.

7 The Neoproterozoic roots of the Front Range

Our thermal history analysis of thermochronologic data from the Front Range, and associated sensitivity tests, provide insight into the thermal history experienced by, and recorded within, the crystalline basement rocks of the range throughout late Proterozoic and Phanerozoic time. Absent accompanying stratigraphic evidence, the geologic significance of this history must be inferred from the duration, peak temperatures, and timing of thermal events constrained by the inversion results. The long duration (at least 18 Myr, and 76 Myr on average) and peak temperature (T_p = 240-285°C) of post-Tava heating (Fig. 5a) implies that Neoproterozoic heating was driven by processes that operate on geologic timescales, rather than short transient thermal events. We discuss the implications of these results for the burial and exhumation history of the Front Range in Neoproterozoic time.

7.1 Neoproterozoic rifting in the Front Range

The duration, magnitude, and timing of the thermal event preserved in the range front, combined with the limited available geologic evidence, suggests that sedimentary burial is the process most likely responsible for heating the basement rocks of the Front Range in late Neoproterozoic time (Fig. 9a, b). Geologic evidence that supports burial in an extensional tectonic setting includes the Tava bodies, because basement-hosted clastic dikes are commonly associated with continental rifts (Fig. 1a; Beacom et al., 1999; Friese et al., 2010; Jonk et al., 2004). This association arises because rift-related crustal extension and concomitant rapid sedimentation are thought to facilitate the fracture opening and fluid overpressure needed for sand remobilization and injection (Jolly & Lonergan, 2002; Jonk, 2010). Although rift-basins are also commonly associated with near-surface hydrothermal systems (Hannington et al., 2005), such as that proposed to be coeval with Tava formation in the Williams Fork Range, ~50 km west of our study area (Jensen et al., 2018), such hydrothermal systems are too short-lived to explain the long-duration heating documented by our samples (Cathles et al., 1997; Henry et al., 1997; Jess et al., 2021).

This article is protected by copyright. All rights reserved.

Author Manuscript

We use the post-Tava T_p to estimate the depth of the sedimentary fill deposited above our range front samples to assess the scale of the proposed rift basin. Assuming a geothermal gradient of 30-50 °C/km and a sample depth below the base of the sedimentary basin of 0-2 km yields basin depths between 3 and 9 km (Text S3). These values are compatible with the sediment accommodation, geothermal gradient, and timescales of thermal subsidence expected in intracontinental rift provinces (Friedmann & Burbank, 1995). We note that modern and ancient analogs for continental rift basins (e.g., the proximal domain of Peron-Pinvidic et al., 2013) clearly document that rift settings are characterized by wedge-shaped sedimentary packages, which are deposited in spatially variable asymmetrical basins that are narrow (20-40 km) and deep (Friedmann & Burbank, 1995). Simple scaling relationships between maximum normal-fault throw and length predict that an extensional system bounding a 3-9 km deep basin would have been tens to hundreds of kilometers long (Kim & Sanderson, 2005; Scholz & Contreras, 1998), consistent with the evolution of a basin along a major crustal structure.

The inference that the rocks of the central Front Range were buried in Neoproterozoic time by a major rift basin is consistent with previous hypotheses that modern Laramide-style ranges have roots in the rifting of western Laurentia during the breakup of supercontinent Rodinia (e.g., Marshak et al., 2000). Therefore, our thermal history analysis provides new constraints on the eastern extent of rift-related extensional faulting (Fig. 1a). Our findings also add to a growing body of stratigraphic, magmatic, and thermochronologic evidence for Rodinia breakup-related tectonism throughout the intermontane western US (C M Dehler et al., 2010; Harlan et al., 2003; Karlstrom et al., 2000; Kingsbury-Stewart et al., 2013; Lund et al., 2003; Sanders et al., 2006)previous hypotheses that the distribution, orientation, and size of Laramide-ranges are linked to pre-existing Proterozoic crustal weaknesses, many potentially generated during the rifting of Rodinia (Marshak et al., 2000; Weil & Yonkee, 2023). Thermochronologic evidence of these linkages, such as ours, is significant because limited stratigraphic evidence directly supports the inversion or reactivation of Proterozoic structures during the Laramide orogeny (e.g., Schmidt & O'Neill, 1982) the inversion of the Uinta basin is perhaps the best-preserved example (e.g., Carol M Dehler et al., 2005). Thermochronologic data have previously been interpreted to document the Laramide reactivation of a Proterozoic fault in New Mexico (Sanders et al., 2006), and our thermal history analysis provides additional evidence of potential reactivation of a Neoproterozoic fault in the vicinity of the Laramide Front Range, thus growing the body of evidence for structural inheritance as a key factor that influenced the style and distribution of deformation during the Laramide orogeny (Marshak et al., 2000).

Overall, our results establish a spatial link between Neoproterozoic extension and Laramide shortening that bolsters previous geometric arguments for a genetic connection between Proterozoic orogenesis and the extent of later Phanerozoic tectonism (Figs. 9c, d; Chapin et al., 2014; Marshak et al., 2000) and are consistent with observations of the Laramide reactivation of individual Neoproterozoic structures (e.g., Luther et al., 2012; Sanders et al., 2006; Wawrzyniec et al., 2007).

This article is protected by copyright. All rights reserved.

Author Manuscript

7.2 Timing and cause of Proterozoic to Phanerozoic Front Range exhumation

Whereas the protracted rifting and subsidence of western Laurentia provides a parsimonious mechanism for Neoproterozoic heating of our samples, our geologic interpretation also requires that the basement rocks were subsequently exhumed to the surface by the time of Cambrian and/or Pennsylvanian deposition on the Great Unconformity. The process(es) responsible for this kilometer-scale erosion are more difficult to ascertain, in part because the timing of exhumation is poorly constrained by our thermal history analysis (Fig. 7). Kilometer-scale erosion on 10-100 Myr timescales requires substantial topographic relief, weak and thus erodible rocks, or a combination of the two. At least three candidate events could be responsible for this exhumation (from most recent to oldest): (1) local shortening-driven rock uplift and exhumation during the ARM orogeny ca. 320-280 Ma; (2) regional post-rifting topographic evolution of the Laurentian passive margin after the final stages of Rodinia breakup at ca. 570-540 Ma (Whitmeyer & Karlstrom, 2007; Yonkee et al., 2014); and (3) glacial or tectonic-driven erosion during Cryogenian-Ediacaran time (Keller et al., 2019; McDannell et al., 2022b; Wang et al., 2023). These candidate events are variably supported by our thermal history results, depending on the geologic constraints incorporated into the models. As such, discriminating among these potential drivers of exhumation is largely dependent on geologic evidence.

7.2.1 Potential for ARM-related exhumation

Several sensitivity test results (Figs. 7b,c) support late Paleozoic, instead of Cambrian, timing for exhumation in the central Front Range. A corollary of this timing is that the >3 km of Neoproterozoic strata that we infer buried our samples, together with any overlying Paleozoic rocks, should have remained intact until the onset of shortening and basement unroofing during the late-Paleozoic ARM orogeny (ca. 320-280 Ma). The ARM is a known, if enigmatic, major tectonic event (Kluth and Coney, 1981; Leary et al., 2017) documented in the Front Range by deposition of the Fountain Formation (Sweet & Soreghan, 2010). This dominantly clastic unit contains material shed from local ARM topographic highs, which was deposited nonconformably on basement rocks in the central Front Range (Fig. 3).

However, there are no geologic observations that support the unroofing of a major Neoproterozoic basin in the Front Range region during the ARM orogeny. Such an interpretation requires a sink for a large volume of exhumed and eroded Neoproterozoic rift strata, but detrital zircon records from the Fountain Formation and other late Paleozoic strata do not reflect a contribution from Tava-like Neoproterozoic sources (Siddoway & Gehrels, 2014) and instead indicate that clastic contributions to the Fountain Formation were locally derived from Yavapai-Mazatzal-dominated source areas (Sharman et al., 2018; T. M. Smith et al., 2023). Although the Fountain Formation in the southern Front Range contains clasts of basement-derived granite and gneiss, as well as recycled cobbles and boulders of the Cambrian Sawatch Formation (which lies nonconformably on basement rocks across the Front Range in the present-day, Fig. 2a), there is a lack of sedimentary detritus as would be expected if Neoproterozoic basin sediments were exhumed at this time (Sweet & Soreghan, 2010). We interpret the absence of Neoproterozoic

This article is protected by copyright. All rights reserved.

Author Manuscript

strata in the Southern Rocky Mountains east of the Uinta Mountains (Fig. 1a) and the absence of recycled Neoproterozoic sources in the Fountain Formation to point to a more regionally extensive driver of exhumation that preceded the ARM orogeny.

7.2.2 Potential for rift-to-drift driven exhumation in latest Neoproterozoic to early Cambrian time

In the thermal history inversion from the range front (Fig. 5a), and variations on this result that assume Cambrian strata were deposited on basement rocks in the central Front Range (e.g., Fig. 7a), the erosion of Neoproterozoic strata occurs prior to ca. 500 Ma. This geologic history requires that the rift-basin strata that buried the Front Range basement were eroded away within ~40 Myr of the final stages of Rodinia breakup ca. 570-540 Ma (Whitmeyer & Karlstrom, 2007; Yonkee et al., 2014) and prior to deposition of the Sauk sequence (Sloss 1963), which is represented in central Colorado by deposition of the late Cambrian Sawatch Formation(Myrow 2003).

The creation of kilometer-scale relief at 10-100 Myr timescales following continental rifting has been inferred globally after Pangaea breakup, although the mechanisms driving burial, exhumation, and topographic evolution at young passive margins are not well understood (P. F. Green et al., 2018; Japsen et al., 2012). The magnitude of erosion associated with post-rift topography appears to be spatially variable but synchronous at regional (e.g., Fame et al., 2018; Wildman et al., 2015) and continental scales (P. F. Green et al., 2018). This synchroneity has been inferred to arise from lithosphere-scale drivers—such as mantle convection localized at the rift margin or changes in plate motions—of relief generation and geomorphic change along passive margins and the exhumation and retreat of passive margin escarpments (e.g., Braun & Beek, 2004).

If exhumation across the Front Range occurred ca. 540-510 Ma, this would broadly correspond with the emergence of the Transcontinental Arch (Brennan et al., 2021; Carlson, 1999), a regional drainage divide (Fig. 1a) that is inferred to have disrupted continent-scale river systems that delivered Grenville-sourced sediment to the western margin of Laurentia (G. Gehrels & Pecha, 2014; Linde et al., 2014; Yonkee et al., 2014). Despite the correspondence in timing between the emergence of the Transcontinental Arch and the timing of exhumation permitted in several of our thermal models and sensitivity tests, the uniformity in the thickness of basal Cambrian deposition across vast regions of Laurentia is difficult to reconcile with large-scale uplift and erosion around this time (Brennan et al., 2021).

7.2.3 Potential for exhumation driven by Neoproterozoic glaciation

Finally, late Neoproterozoic time was also characterized by global glaciations that have been hypothesized to denude the continents by an average of 3-5 km (Keller et al., 2019). Our range front inversion (Fig. 5a) is consistent with this magnitude of exhumation in Cryogenian time, so long as it occurs after ca. 700 Ma. The stratigraphic record of western Laurentia documents at least two major Neoproterozoic glaciations, commonly associated with Snowball

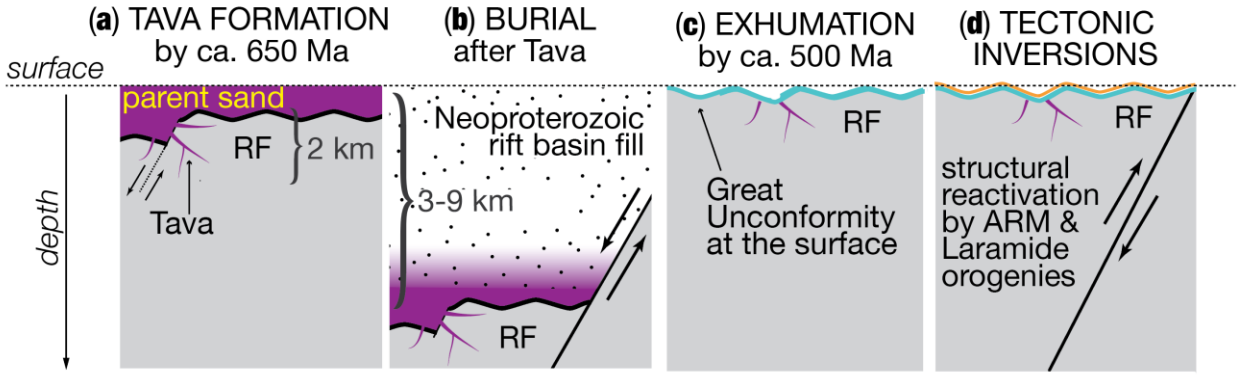
This article is protected by copyright. All rights reserved.

Author Manuscript

Earth conditions (Macdonald et al., 2013). For example, in eastern California the Cryogenian Kingston Peak Formation preserves diamictites and cap carbonates associated with both the Sturtian and Marinoan glaciations (Nelson et al., 2020; Petterson et al., 2011). In the stratigraphically younger Johnnie Formation, a major intra-formational incision event is coeval with the Gaskiers glaciation (ca. 580 Ma; Witkosky & Wernicke, 2018), although attribution of this incision to glacial versus tectonic drivers is debated (Clapham & Corsetti, 2005; Giles et al., 2023). Although stratigraphic evidence for the earlier two glacial episodes in western Laurentia is unquestioned, the Neoproterozoic stratigraphic record overall reflects complex contributions of both glaciation and active rifting (LeHeron et al., 2018); either, or both, processes could be reasonably invoked to lower regional base level (via glacial drawdown or tectonic subsidence, respectively) and drive exhumation across the continental margin. Recent studies that have reported low sedimentation rates in western Laurentia associated with Cryogenian glacial periods (e.g., Anttila et al., 2024) may favor a tectonic driver for exhumation of the Front Range region in Cryogenian time. However, our results lack the temporal resolution to distinguish among discrete glacial events, and they also cannot be used to refute alternative interpretations that attribute post-Tava exhumation to non-glacial processes in Neoproterozoic or Paleozoic time.

7.3 Spatial extent of observed Neoproterozoic thermal history

We emphasize that the Neoproterozoic history we resolve for the central Front Range need not be true for the northern or southern Front Range. Indeed, despite the non-uniqueness of many published ZHe datasets from this region, it is reasonable to expect that deep-time thermochronology may be capable of resolving *tT* history variations that arise from Proterozoic processes on spatial scales similar to those which are observed in Cenozoic continental rifts and orogenic systems (i.e., tens of kilometers). However, we have also demonstrated how suites of samples from Proterozoic rocks will vary in their sensitivity to specific deep-time thermal histories, even given the same modeling choices (e.g., the difference between our divide and range front samples, Fig. 5). As such, the spatial resolution of deep-time thermochronologic studies will likely be constrained by the availability of sample suites sensitive to such deep-time histories.



This article is protected by copyright. All rights reserved.

Figure 9. *Our proposed geologic history of the Front Range reflects the rift-to-drift evolution of western Laurentia. RF—range front.* ***(a)*** *The Tavakaiv (Tava) quartzite formed within ~2 km of the Neoproterozoic paleosurface. The emplacement of these basement-hosted clastic bodies is likely associated with extension accompanying rifting of the supercontinent Rodinia.* ***(b)*** *After Tava emplacement, basement rocks reached 240-285°C in the hanging wall of a deep basin formed during intracontinental rifting.* ***(c)*** *By ca. 500 Ma, basement rocks returned to the near surface via exhumation of the western Laurentian passive margin driven by post-rift lithospheric processes and/or global "Snowball Earth" glaciation. As discussed in the text, the timing of this rock cooling, and thus the process responsible for this exhumation, is poorly constrained by our results.* ***(d)*** *Our results support previous inferences* (Chapin et al., 2014; e.g., Marshak et al., 2000) *that the Front Range, and likely other Laramide ranges, are inverted Proterozoic rift structures that were reactivated and accommodated crustal shortening and surface uplift during the Ancestral Rocky Mountains (ARM) and Laramide orogenies.*

8 Conclusions

We analyze ZHe data from Paleoproterozoic basement rocks of the central Front Range (Murray, Niemi, et al., 2022) and assess how thermal history models that incorporate these data resolve the deep-time tectonic history of the eastern edge of the modern Rocky Mountains. We use sensitivity testing to evaluate the geologic significance of the results and compare our work to other recent interpretations of ZHe data from the Front Range (Flowers et al., 2020; Havranek & Flowers, 2022; McDannell et al., 2022b; Ricketts et al., 2021). Our thermal history analysis also addresses an ongoing debate regarding methods for modeling and interpreting thermochronologic data in deep time.

One suite of samples has a ZHe age-[*eU*] trend that, when paired with AHe data, published $^{40}Ar/^{39}Ar$ data (Shaw et al., 1999), and field relationships, documents significant Neoproterozoic heating to 240-285˚C. Sensitivity tests confirm that this reheating is resolved because fitting a ca. 61 ± 7.5 Ma ZHe age pediment, along with the older low-[*eU*] ZHe ages and biotite Ar ages, requires the annealing of radiation damage in zircon that accumulated earlier in Proterozoic time. We argue that the magnitude (240-285˚C) and duration (>18 Myr) of Neoproterozoic heating and subsequent cooling is well constrained by our thermal history results. We attribute this heating event to 3-9 km of burial in a major extensional basin formed during the rifting of supercontinent Rodinia. This interpretation places the Front Range within the rifted margin of western Laurentia and supports existing hypotheses regarding the Proterozoic origin of the Front Range and other basement-cored uplifts most recently exhumed during the Laramide orogeny (Marshak et al., 2000).

Improved constraints on the timing of post-rifting exhumation in the Front Range region, above and beyond those provided by our thermal history analysis, are necessary to genetically link this significant erosional event to tectonic or glacial drivers. Such improvements will arise from the refinement of models of radiation damage accumulation and annealing on He mobility in zircon grains, as well as from new temporal constraints on the geologic relationships that underpin deep-time thermal history models. In particular, the potential for young, high-[*eU*]

This article is protected by copyright. All rights reserved.

Author Manuscript

zircon grains to offer key constraints on Proterozoic *tT* histories underscores the exciting advances in our understanding of Proterozoic tectonics that could be in store with continued refinement of the empirical calibration of radiation-damage effects in highly damaged zircon grains. Nonetheless, our thermal history analysis offers the first quantitative evidence of kilometer-scale late Neoproterozoic burial and later exhumation of basement rocks in the Front Range region and therefore supporting the hypothesis that the Laramide Rocky Mountains formed by the inversion of a Rodinian rift zone and underscoring the growing utility of low-temperature thermochronology for quantifying the geologic processes that operated along active continental margins during Proterozoic time.

Acknowledgements

KEM acknowledges support from Idaho State University and the University of Michigan, as well as funding from NSF-EAR-2140480. MKC and NAN acknowledge support from NSF-EAR-1151247, research funds from the University of Michigan, and CIRES Sabbatical Fellowships from CU Boulder. We thank E. Portenga and S. Gallen for field assistance and A. Maslyn for laboratory support. Detrital zircon U/Pb analyses of the Tava were generously provided by C.S. Siddoway and supported by Colorado College institutional grants; the Arizona LaserChron Center (NSF-EAR-1649254) supported the zircon U/Pb analyses. Thanks to A. Ault, D. Orme, A. Stevens Goddard and A. Abbey for discussions of thermal history modeling and to C. Siddoway for Tava discussions and comments on an early version of this manuscript. Comments from four anonymous reviewers improved earlier versions of this work. We thank R. Flowers, one anonymous reviewer, and the Associate Editor for helpful guidance on this work.

Open Research

Thermochronologic data from Murray, Niemi, et al. (2022) and Shaw et al. (1999) were used in this work. Additional data, included in the supplementary materials in this submitted manuscript for the review process, will be made available with a persistent doi identifier via the University of Michigan's Deep Blue Repository. Version 1.9.3 of the software HeFTy was used for inverse thermal history modeling and is included in this paper by Ketcham (2005). Version 1 of W. R. Guenthner's RDAAM code (Guenthner, 2021) was used for forward modeling and is available at https://github.com/wrguenthner/DAAM.

References

Anttila, E. S. C., Macdonald, F. A., Zinto, J., & Britt, M. D. (2024). The Real McCoy: Great Unconformity source-to-sink on the rifted passive margin of Laurentia. *Earth and Planetary Science Letters, 642*, 118852. https://doi.org/10.1016/j.epsl.2024.118852

This article is protected by copyright. All rights reserved.

Author Manuscript

Author Manuscript

Ault, A. K., Guenthner, W. R., Moser, A. C., Miller, G. H., & Refsnider, K. A. (2018). Zircon grain selection reveals (de)coupled metamictization, radiation damage, and He diffusivity. *Chemical Geology*, *490*, 1–12. https://doi.org/10.1016/j.chemgeo.2018.04.023

Beacom, L. E., Anderson, T. B., & Holdsworth, R. E. (1999). Using basement-hosted clastic dykes as syn-rifting palaeostress indicators: An example from the basal Stoer Group, northwest Scotland, *136*(3), 301–310. https://doi.org/10.1017/s0016756899002605

Braun, J., & Beek, P. V. D. (2004). Evolution of passive margin escarpments: What can we learn from low-temperature thermochronology? *Journal of Geophysical Research-Earth Surface*, *109*. https://doi.org/10.1029/2004fj000147

Brennan, D. T., Mitchell, R. N., Spencer, C. J., Murphy, J. B., & Li, Z. (2021). A tectonic model for the Transcontinental Arch: Progressive migration of a Laurentian drainage divide during the Neoproterozoic–Cambrian Sauk Transgression. *Terra Nova*, *33*(4), 430–440. https://doi.org/10.1111/ter.12528

Caine, J. S., Nelson, E. P., Beach, S. T., & Layer, P. W. (2006). Structural Fabrics, Mineralization, and Laramide Kinematics of the Idaho Springs-Ralston Shear Zone, Colorado Mineral Belt and Central Front Range Uplift. *The Mountain Geologist*, *43*(1), 1–24.

Caine, J. S., Ridley, J., & Wessel, Z. R. (2010). To reactivate or not to reactivate—Nature and varied behavior of structural inheritance in the Proterozoic basement of the eastern Colorado Mineral Belt over 1.7 billion years of earth history. In L. A. Morgan & S. L. Quane (Eds.) (pp. 119–140). Geological Society of America. https://doi.org/10.1130/2010.0018(06)

Carlson, M. P. (1999). Transcontinental Arch — a pattern formed by rejuvenation of local features across central North America. *Tectonophysics*, *305*(1), 225–233. https://doi.org/10.1016/s0040-1951(99)00005-0

Cathles, L. M., Erendi, A. H. J., & Barrie, T. (1997). How long can a hydrothermal system be sustained by a single intrusive event? *Economic Geology*, *92*(7–8), 766–771. https://doi.org/10.2113/gsecongeo.92.7-8.766

Chapin, C. E. (2012). Origin of the Colorado Mineral Belt. *Geosphere*, *8*(1), 28–43. https://doi.org/10.1130/ges00694.1

Chapin, C. E., Kelley, S. A., & Cather, S. M. (2014). The Rocky Mountain Front, southwestern USA. *Geosphere*, *10*(5), 1043–1060. https://doi.org/10.1130/ges01003.1

Clapham, M. E., & Corsetti, F. A. (2005). Deep valley incision in the terminal Neoproterozoic (Ediacaran) Johnnie Formation, eastern California, USA: Tectonically or glacially driven? *Precambrian Research*, *141*(3–4), 154–164. https://doi.org/10.1016/j.precamres.2005.09.002

This article is protected by copyright. All rights reserved.

Cole, J. C., & Braddock, W. A. (2009). *Geologic Map of the Estes Park 30' x 60' Quadrangle, North-Central Colorado* (U.S. Geological Survey Scientific Investigations Map 3000) (p. 56). Retrieved from https://pubs.usgs.gov/sim/3039/downloads/SIM_3039_Pamphlet.pdf

Corsetti, F. A., & Grotzinger, J. P. (2005). Origin and Significance of Tube Structures in Neoproterozoic Post-glacial Cap Carbonates: Example from Noonday Dolomite, Death Valley, United States. *PALAIOS*, *20*(4), 348–362. https://doi.org/10.2110/palo.2003.p03-96

Courtney-Davies, L., Flowers, R. M., Siddoway, C. S., Tasistro-Hart, A., & Macdonald, F. A. (2024). Hematite U-Pb dating of Snowball Earth meltwater events. *Proceedings of the National Academy of Sciences*, *121*(47), e2410759121. https://doi.org/10.1073/pnas.2410759121

Cross, W. (1894). Intrusive sandstone dikes in granite. *Geological Society of America Bulletin*, *5*(1), 225–230. https://doi.org/10.1130/gsab-5-225

Dehler, C M, Fanning, C. M., Link, P. K., Kingsbury, E. M., & Rybczynski, D. (2010). Maximum depositional age and provenance of the Uinta Mountain Group and Big Cottonwood Formation, northern Utah: Paleogeography of rifting western Laurentia. *Geological Soceity of America Bulletin*, *122*(9–10), 1686–1699. https://doi.org/10.1130/b30094.1

Dehler, Carol M, Sprinkel, D. A., & Porter, S. M. (2005). GSA Field Guide 6: Interior Western United States, 1–25. https://doi.org/10.1130/2005.fld006(01)

Fame, M. L., Spotila, J. A., Owen, L. A., Dortch, J. M., & Shuster, D. L. (2018). Spatially heterogeneous post-Caledonian burial and exhumation across the Scottish Highlands. *Lithosphere*, *10*(3), 406–425. https://doi.org/10.1130/l678.1

Flowers, R. M., Ketcham, R. A., Shuster, D. L., & Farley, K. A. (2009). Apatite (U–Th)/He thermochronometry using a radiation damage accumulation and annealing model. *Geochimica et Cosmochimica Acta*, *73*(8), 2347–2365. https://doi.org/10.1016/j.gca.2009.01.015

Flowers, R. M., Farley, K. A., & Ketcham, R. A. (2015). A reporting protocol for thermochronologic modeling illustrated with data from the Grand Canyon. *Earth And Planetary Science Letters*, *432*(C), 425–435. https://doi.org/10.1016/j.epsl.2015.09.053

Flowers, R. M., Macdonald, F. A., Siddoway, C. S., & Havranek, R. (2020). Diachronous development of Great Unconformities before Neoproterozoic Snowball Earth. *Proceedings of the National Academy of Sciences*, *117*(19), 10172–10180. https://doi.org/10.1073/pnas.1913131117

Flowers, R. M., Ketcham, R. A., Macdonald, F. A., Siddoway, C. S., & Havranek, R. E. (2022). Existing thermochronologic data do not constrain Snowball glacial erosion below the Great

This article is protected by copyright. All rights reserved.

Author Manuscript

Unconformities. *Proceedings of the National Academy of Sciences*, *119*(38), e2208451119. https://doi.org/10.1073/pnas.2208451119

Friedmann, S. J., & Burbank, D. W. (1995). Rift basins and supradetachment basins: Intracontinental extensional end-members. *Basin Research*, *7*, 109–127.

Friese, N., Vollbrecht, A., Leiss, B., & Jacke, O. (2010). Cambrian sedimentary dykes in the Proterozoic basement of the Västervik area (southeast Sweden): episodic formation inferred from macro- and microfabrics. *International Journal of Earth Sciences*, *100*(4), 741–752. https://doi.org/10.1007/s00531-009-0508-3

Gallagher, K. (2012). Transdimensional inverse thermal history modeling for quantitative thermochronology. *Journal of Geophysical Research*, *117*(B2), B02408. https://doi.org/10.1029/2011jb008825

Gautheron, C., Tassan-Got, L., Barbarand, J., & Pagel, M. (2009). Effect of alpha-damage annealing on apatite (U–Th)/He thermochronology. *Chemical Geology*, *266*(3–4), 157–170. https://doi.org/10.1016/j.chemgeo.2009.06.001

Gehrels, G., & Pecha, M. (2014). Detrital zircon U-Pb geochronology and Hf isotope geochemistry of Paleozoic and Triassic passive margin strata of western North America. *Geosphere*, *10*(1), 49–65. https://doi.org/10.1130/ges00889.1

Gehrels, G. E., Valencia, V. A., & Ruiz, J. (2008). Enhanced precision, accuracy, efficiency, and spatial resolution of U-Pb ages by laser ablation-multicollector-inductively coupled plasma-mass spectrometry. *Geochemistry Geophysics Geosystems*, *9*(3), Q03017. https://doi.org/10.1029/2007gc001805

Giles, S. M., Christie-Blick, N., & Lankford-Bravo, D. F. (2023). A subaerial origin for the mid-Ediacaran Johnnie valleys, California and Nevada: Implications for a diachronous onset of the Shuram excursion. *Precambrian Research*, *397*, 107187. https://doi.org/10.1016/j.precamres.2023.107187

Ginster, U., Reiners, P. W., Nasdala, L., & N, C. C. (2019). Annealing kinetics of radiation damage in zircon. *Geochimica et Cosmochimica Acta*, *249*, 225–246. https://doi.org/10.1016/j.gca.2019.01.033

Green, G. N. (1992). *The Digital Geologic Map of Colorado in ARC/INFO Format* (U.S. Geological Survey Open-File Report - No. 92–0507) (p. 9). Retrieved from http://pubs.usgs.gov/of/1992/ofr-92-0507/

Green, P. F., Japsen, P., Chalmers, J. A., Bonow, J. M., & Duddy, I. R. (2018). Post-breakup burial and exhumation of passive continental margins: Seven propositions to inform geodynamic models. *Gondwana Research*, *53*(C), 58–81. https://doi.org/10.1016/j.gr.2017.03.007

This article is protected by copyright. All rights reserved.

Author Manuscript

Guenthner, W. R. (2021). Implementation of an Alpha Damage Annealing Model for Zircon (U-Th)/He Thermochronology With Comparison to a Zircon Fission Track Annealing Model. *Geochemistry, Geophysics, Geosystems*, *22*(2). https://doi.org/10.1029/2019gc008757

Guenthner, W. R., Reiners, P. W., Ketcham, R. A., Nasdala, L., & Giester, G. (2013). Helium diffusion in natural zircon: Radiation damage, anisotropy, and the interpretation of zircon (U-Th)/He thermochronology. *American Journal Of Science*, *313*(3), 145–198. https://doi.org/10.2475/03.2013.01

Hannington, M. D., Ronde, C. E. J. D., & Petersen, S. (2005). Sea-Floor Tectonics and Submarine Hydrothermal Systems. In J. W. Hedenquist, J. F. H. Thompson, R. J. Goldfarb, & J. P. Richards (Eds.), *One Hundredth Anniversary Volume*. https://doi.org/10.5382/av100.06

Harlan, S. S., Heaman, L., LeCheminant, A. N., & Premo, W. R. (2003). Gunbarrel mafic magmatic event: A key 780 Ma time marker for Rodinia plate reconstructions. *Geology*, *31*(12), 1053–1056. https://doi.org/10.1130/g19944.1

Harrison, T. M. (1981). Diffusion of 40Ar in hornblende. *Contributions to Mineralogy and Petrology*, *78*, 324–331.

Havranek, R. E., & Flowers, R. M. (2022). Zircon (U-Th)/He data for the Colorado Front Range "fourteeners" and testing Cryogenian exhumation of sub-Great Unconformity basement. *Chemical Geology*, *591*, 120702. https://doi.org/10.1016/j.chemgeo.2021.120702

Henry, C. D., Elson, H. B., McIntosh, W. C., Heizler, M. T., & Castor, S. B. (1997). Brief duration of hydrothermal activity at Round Mountain, Nevada, determined from Ar 40 /Ar 39 geochronology. *Economic Geology*, *92*(7–8), 807–826. https://doi.org/10.2113/gsecongeo.92.7-8.807

Hoffman, P. F., Abbot, D. S., Ashkenazy, Y., Benn, D. I., Brocks, J. J., Cohen, P. A., et al. (2017). Snowball Earth climate dynamics and Cryogenian geology-geobiology. *Science Advances*, *3*(11), e1600983. https://doi.org/10.1126/sciadv.1600983

Howard, J. E. (1966). Patterns of Sediment Dispersal in the Fountain Formation of Colorado. *The Mountain Geologist*, *3*(4), 147–153.

Hurst, A., Scott, A., & Vigorito, M. (2011). Physical characteristics of sand injectites. *Earth Science Reviews*, *106*(3–4), 215–246. https://doi.org/10.1016/j.earscirev.2011.02.004

Japsen, P., Chalmers, J. A., Green, P. F., & Bonow, J. M. (2012). Elevated, passive continental margins: Not rift shoulders, but expressions of episodic, post-rift burial and exhumation. *Global and Planetary Change*, *90–91*(C), 73–86. https://doi.org/10.1016/j.gloplacha.2011.05.004

Jensen, J. L., Siddoway, C. S., Reiners, P. W., Ault, A. K., Thomson, S. N., & Steele-MacInnis, M. (2018). Single-crystal hematite (U–Th)/He dates and fluid inclusions document

This article is protected by copyright. All rights reserved.

Author Manuscript

widespread Cryogenian sand injection in crystalline basement. *Earth And Planetary Science Letters*, *500*, 145–155. https://doi.org/10.1016/j.epsl.2018.08.021

Jess, S., Enkelmann, E., Grasby, S. E., & Fraser, K. (2021). Determining the Lifespan of Hydrothermal Systems Using Thermochronology and Thermal Modeling. *Journal of Geophysical Research: Earth Surface*, *126*(11). https://doi.org/10.1029/2021jf006286

Johnson, J. E., Flowers, R. M., Baird, G. B., & Mahan, K. H. (2017). "Inverted" zircon and apatite (U–Th)/He dates from the Front Range, Colorado: High-damage zircon as a low-temperature (<50 °C) thermochronometer. *Earth And Planetary Science Letters*, *466*, 80–90. https://doi.org/10.1016/j.epsl.2017.03.002

Jolly, R. J. H., & Lonergan, L. (2002). Mechanisms and controls on the formation of sand intrusions. *Journal of the Geological Society*, *159*(5), 605–617. https://doi.org/10.1144/0016-764902-025

Jonk, R. (2010). Sand-rich injectites in the context of short-lived and long-lived fluid flow. *Basin Research*, *22*(4), 603–621. https://doi.org/10.1111/j.1365-2117.2010.00471.x

Jonk, R., Kelly, J., & Parnell, J. (2004). The origin and tectonic significance of Lewisian- and Torridonian-hosted clastic dykes near Gairloch, NW Scotland. *Scottish Journal of Geology*, *40*(2), 123–130. https://doi.org/10.1144/sjg40020123

Karlstrom, K. E., Harlan, S. S., Williams, M. L., McLelland, J., Geissman, J. W., & Åhäll, K. I. (1999). Refining Rodinia: Geologic evidence for the Australia-Western U.S. Connection in the Proterozoic. *GSA Today*, *9*(10), 2–7.

Karlstrom, K. E., Bowring, S. A., Dehler, C. M., Knoll, A. H., Porter, S. M., Marais, D. J. D., et al. (2000). Chuar Group of the Grand Canyon: Record of breakup of Rodinia, associated change in the global carbon cycle, and ecosystem expansion by 740 Ma. *Geology*, *28*(7), 619–622. https://doi.org/10.1130/0091-7613(2000)28<619:cgotgc>2.0.co;2

Kauffman, E. G. (1977). Geological and biological overview: Western Interior Cretaceous basin. *The Mountain Geologist*, *14*(3–4), 75–98.

Kaufman, A. J., Corsetti, F. A., & Varni, M. A. (2007). The effect of rising atmospheric oxygen on carbon and sulfur isotope anomalies in the Neoproterozoic Johnnie Formation, Death Valley, USA. *Chemical Geology*, *237*(1–2), 47–63. https://doi.org/10.1016/j.chemgeo.2006.06.023

Keller, C. B., Husson, J. M., Mitchell, R. N., Bottke, W. F., Gernon, T. M., Boehnke, P., et al. (2019). Neoproterozoic glacial origin of the Great Unconformity. *Proceedings of the National Academy of Sciences*, *116*(4), 1136–1145. https://doi.org/10.1073/pnas.1804350116

Kelley, S. A. (2002). Unroofing of the southern Front Range, Colorado A view from the Denver Basin. *Rocky Mountain Geology*, *37*(2), 189–2000.

This article is protected by copyright. All rights reserved.

Author Manuscript

Kelley, S. A., & Chapin, C. E. (2004). Denudation history and internal structure of the Front Range and Wet Mountains, Colorado, based on apatite fission track thermochronology. *New Mexico Bureau of Geology and Mineral Resources Bulletin*, *160*, 41–78. Retrieved from https://geoinfo.nmt.edu/publications/monographs/bulletins/160/downloads/03kelley.pdf

Kellogg, K. S., Shroba, R. R., Bryant, B., & Premo, W. R. (2008). *Geologic Map of the Denver West 30' x 60' Quadrangle, North-Central Colorado* (U.S. Geological Survey Scientific Investigations Map 3000 No. Map 3000) (pp. 1-48 pamphlet). Retrieved from https://pubs.usgs.gov/sim/3000/downloads/pdf/3000_pamphlet_508.pdf

Ketcham, R. A. (2005). Forward and inverse modeling of low-temperature thermochronometry data. *Reviews in Mineralogy and Geochemistry*, *58*, 275–314. Retrieved from ftp://ftp.ctlab.geo.utexas.edu/Ketcham/ft/HeFTy

Ketcham, R. A. (2024). Thermal history inversion from thermochronometric data and complementary information: New methods and recommended practices. *Chemical Geology*, *653*, 122042. https://doi.org/10.1016/j.chemgeo.2024.122042

Ketcham, R. A., Donelick, R. A., Balestrieri, M. L., & Zattin, M. (2009). Reproducibility of apatite fission-track length data and thermal history reconstruction. *Earth and Planetary Science Letters*, *284*(3–4), 504–515. https://doi.org/10.1016/j.epsl.2009.05.015

Kim, Y.-S., & Sanderson, D. J. (2005). The relationship between displacement and length of faults: a review. *Earth Science Reviews*, *68*(3–4), 317–334. https://doi.org/10.1016/j.earscirev.2004.06.003

Kingsbury-Stewart, E. M., Osterhout, S. L., Link, P. K., & Dehler, C. M. (2013). Sequence stratigraphy and formalization of the Middle Uinta Mountain Group (Neoproterozoic), central Uinta Mountains, Utah: A closer look at the western Laurentian Seaway at ca. 750Ma. *Precambrian Research*, *236*, 65–84. https://doi.org/10.1016/j.precamres.2013.06.015

Lawton, T. F. (2008). *Laramide Sedimentary Basins* (Vol. 5). Elsevier. https://doi.org/10.1016/s1874-5997(08)00012-9

LeHeron, D. P., Busfield, M. E., Ali, D. O., Vandyk, T., & Tofaif, S. (2018). A tale of two rift shoulders, and two ice masses: the Cryogenian glaciated margin of Death Valley, California. In *Special Publications* (Vol. 475, pp. 35–52). Geological Society, London.

Lester, A. P., Larson, E. E., Farmer, G. L., Stern, C. R., & Funk, J. A. (2001). Neoproterozoic kimberlite emplacement in the Front Range, Colorado, *36*(1), 1–12. https://doi.org/10.2113/gsrocky.36.1.1

Linde, G. M., Cashman, P. H., Jr., J. H. T., & Dickinson, W. R. (2014). Stratigraphic trends in detrital zircon geochronology of upper Neoproterozoic and Cambrian strata, Osgood Mountains, Nevada, and elsewhere in the Cordilleran miogeocline: Evidence for early

This article is protected by copyright. All rights reserved.

Author Manuscript

Cambrian uplift of the Transcontinental Arch. *Geosphere*, *10*(6), 1402–1410. https://doi.org/10.1130/ges01048.1

Lovering, T. S., & Goddard, E. N. (1950). Geology and ore deposits of the Front Range Colorado. *US Geological Survey Professional Paper*, *223*.

Lund, K., Aleinikoff, J. N., Evans, K. V., & Fanning, C. M. (2003). SHRIMP U-Pb geochronology of Neoproterozoic Windermere Supergroup, central Idaho: Implications for rifting of western Laurentia and synchroneity of Sturtian glacial deposits. *GSA Bulletin*, *115*(3), 349–372. https://doi.org/10.1130/0016-7606(2003)115<0349:supgon>2.0.co;2

Luther, A., Axen, G., & Cather, S. (2012). Deciphering the early history of a multiply reactivated fault using strain analysis in an adjacent fold: Evidence for early brittle-plastic slip on the Picuris-Pecos fault, New Mexico, USA. *Geosphere*, *8*(3), 703–715. https://doi.org/10.1130/ges00776.1

Macdonald, F. A., Prave, A. R., Petterson, R., Smith, E. F., Pruss, S. B., Oates, K., et al. (2013). The Laurentian record of Neoproterozoic glaciation, tectonism, and eukaryotic evolution in Death Valley, California. *GSA Bulletin*, *125*(7–8), 1203–1223. https://doi.org/10.1130/b30789.1

Mackintosh, V., Kohn, B., Gleadow, A., & Gallagher, K. (2019). Long-term reactivation and morphotectonic history of the Zambezi Belt, northern Zimbabwe, revealed by multi-method thermochronometry. *Tectonophysics*, *750*, 117–136. https://doi.org/10.1016/j.tecto.2018.11.009

Marshak, S., & Paulsen, T. (1996). Midcontinent U.S. fault and fold zones: A legacy of Proterozoic intracratonic extensional tectonism? *Geology*, *24*(2), 151–154. https://doi.org/10.1130/0091-7613(1996)024<0151:musfaf>2.3.co;2

Marshak, S., Karlstom, K., & Timmons, J. M. (2000). Inversion of proterozoic extensional faults: An explanation for the pattern of Laramide and Ancestral rockies intracratonic deformation, United States. *Geology*, *28*(8), 735–738. https://doi.org/10.1130/0091-7613(2000)28<735:iopefa>2.0.co;2

McCoy, A. M., Karlstrom, K. E., Shaw, C. A., & Williams, M. L. (2005). *The Proterozoic Ancestry of the Colorado Mineral Belt: 1.4 Ga Shear Zone System in Central Colorado* (Vol. 154). American Geophysical Union. https://doi.org/10.1029/154gm06

McDannell, K. T., & Flowers, R. M. (2020). Vestiges of the Ancient: Deep-Time Noble Gas Thermochronology. *Elements*, *16*(5), 325–330. https://doi.org/10.2138/gselements.16.5.325

McDannell, K. T., Keller, C. B., Guenthner, W. R., Zeitler, P. K., & Shuster, D. L. (2022a). Reply to Flowers et al.: Existing thermochronologic data constrain Snowball glacial erosion below the Great Unconformity. *Proceedings of the National Academy of Sciences*, *119*(38), e2209946119. https://doi.org/10.1073/pnas.2209946119

This article is protected by copyright. All rights reserved.

Author Manuscript

McDannell, K. T., Keller, C. B., Guenthner, W. R., Zeitler, P. K., & Shuster, D. L. (2022b). Thermochronologic constraints on the origin of the Great Unconformity. *Proceedings of the National Academy of Sciences of the United States of America*, *119*(5), e2118682119. https://doi.org/10.1073/pnas.2118682119

McDougall, I., & Harrison, T. M. (1999). *Geochronology and Thermochronology by the 40Ar/39Ar Method*. Oxford University Press.

Murray, K. E., Orme, D. A., & Reiners, P. W. (2014). Effects of U–Th-rich grain boundary phases on apatite helium ages. *Chemical Geology*, *390*, 135–151. https://doi.org/10.1016/j.chemgeo.2014.09.023

Murray, K. E., Niemi, N. A., & Clark, M. C. (2022). *Apatite and Zircon (U-Th)/He Thermochronometry Data from the Colorado Front Range, Boulder County, Colorado, USA [Data set]*. University of Michigan - Deep Blue Data. Retrieved from https://doi.org/10.7302/g4eg-vr84

Murray, K. E., Stevens Goddard, A. L., Abbey, A. L., & Wildman, M. (2022). Thermal history modeling techniques and interpretation strategies: Applications using HeFTy. *Geosphere*, *18*(5), 1622–1642. https://doi.org/10.1130/ges02500.1

Nelson, L. L., Smith, E. F., Hodgin, E. B., Crowley, J. L., Schmitz, M. D., & Macdonald, F. A. (2020). Geochronological constraints on Neoproterozoic rifting and onset of the Marinoan glaciation from the Kingston Peak Formation in Death Valley, California (USA). *Geology*, *48*(11), 1083–1087. https://doi.org/10.1130/g47668.1

Nesse, W. D. (2006). Geometry and Tectonics of the Laramide Front Range, Colorado. *The Mountain Geologist*, *43*(1), 25–44. Retrieved from http://archives.datapages.com/data/mountain-geologist-rmag/data/043/043001/pdfs/25.pdf

Orme, D. A., Guenthner, W. R., Laskowski, A. K., & Reiners, P. W. (2016). Long-term tectonothermal history of Laramide basement from zircon–He age-eU correlations. *Earth And Planetary Science Letters*, *453*, 119–130. https://doi.org/10.1016/j.epsl.2016.07.046

Peron-Pinvidic, G., Manatschal, G., & Osmundsen, P. T. (2013). Structural comparison of archetypal Atlantic rifted margins: A review of observations and concepts. *Marine and Petroleum Geology*, *43*, 21–47. https://doi.org/10.1016/j.marpetgeo.2013.02.002

Peters, S. E., & Gaines, R. R. (2012, April 8). Formation of the 'Great Unconformity' as a trigger for the Cambrian explosion. Retrieved from http://www.nature.com/nature/journal/v484/n7394/pdf/nature10969.pdf

Petterson, R., Prave, A. R., & Wernicke, B. P. (2011). Glaciogenic and related strata of the Neoproterozoic Kingston Peak Formation in the Panamint Range, Death Valley region, California | Geological Society, London, Memoirs. In E. Arnaud, G. P. Halverson, & G.

This article is protected by copyright. All rights reserved.

Author Manuscript

Shields-Zhou (Eds.), *Memoirs* (Vol. 36, pp. 459–465). Geological Society, London. https://doi.org/10.1144/m36.41

Picha, F., & Gibson, R. I. (1985). Cordilleran hingeline: Late Precambrian rifted margin of the North American craton and its impact on the depositional and structural history, Utah and Nevada. *Geology*, *13*(7), 465–468. https://doi.org/10.1130/0091-7613(1985)13<465:chlprm>2.0.co;2

Plummer, P. S. (2024). Evolution and extinction in a supercontinental world: did the breakup of Rodinia provide metazoans with evolutionary salvation? *Australian Journal of Earth Sciences*, *71*(6), 821–831. https://doi.org/10.1080/08120099.2024.2364710

Prave, A. R. (1999). Two diamictites, two cap carbonates, two δ13C excursions, two rifts: The Neoproterozoic Kingston Peak Formation, Death Valley, California. *Geology*, *27*(4), 339–342. https://doi.org/10.1130/0091-7613(1999)027<0339:tdtcct>2.3.co;2

Premo, W. R., & Fanning, C. M. (2000). SHRIMP U-Pb zircon ages for Big Creek gneiss, Wyoming and Boulder Creek batholith, Colorado Implications for timing of Paleoproterozoic accretion of the northern Colorado province. *Rocky Mountain Geology*, *35*(1), 31–50. https://doi.org/10.2113/35.1.31

Raynolds, R. G. (1997). Synorogenic and Post-Orogenic Strata in the Central Front Range, Colorado (pp. 43–48). Rocky Mountain Association of Geologists. Retrieved from http://archives.datapages.com/data/rmag/geohistfrontrange1997/raynolds_b.pdf

Reiners, P. W. (2005). Zircon (U-Th)/He thermochronometry. *Reviews in Mineralogy and Geochemistry*, *58*, 151–179. https://doi.org/10.2138/rmg.2005.58.6

Reiners, P. W., & Brandon, M. T. (2006). Using thermochronology to understand orogenic erosion. *Annual Review of Earth and Planetary Sciences*, *34*(1), 419–466. https://doi.org/10.1146/earth.2006.34.issue-1

Ricketts, J. W., Roiz, J., Karlstrom, K. E., Heizler, M. T., Guenthner, W. R., & Timmons, J. M. (2021). Tectonic controls on basement exhumation in the southern Rocky Mountains (United States): The power of combined zircon (U-Th)/He and K-feldspar 40Ar/39Ar thermochronology. *Geology*. https://doi.org/10.1130/g49141.1

Sanders, R. E., Heizler, M. T., & Goodwin, L. B. (2006). 40Ar/39Ar thermochronology constraints on the timing of Proterozoic basement exhumation and fault ancestry, southern Sangre de Cristo Range, New Mexico. *Geological Soceity of America Bulletin*, *118*(11–12), 1489–1506. https://doi.org/10.1130/b25857.1

Schmidt, C. J., & O'Neill, J. M. (1982). Structural evolution of the southwest Montana transverse zone. In R. B. Powers (Ed.), *Geologic Studies of the Cordilleran Thrust Belt, Vol. 1* (pp. 193–218). Rocky Mountain Association of Geologists.

This article is protected by copyright. All rights reserved.

Scholz, C. H., & Contreras, J. C. (1998). Mechanics of continental rift architecture. *Geology*, *26*(11), 967–970. https://doi.org/10.1130/0091-7613(1998)026<0967:mocra>2.3.co;2

Sharman, G. R., Stockli, D. F., Flaig, P. P., Raynolds, R. G., & Covault, J. A. (2018). Local-to-distant provenance cyclicity of the southern Front Range, central Colorado: Insights from detrital zircon geochronology. In R. V. Ingersoll, T. F. Lawton, & S. A. Graham (Eds.), *Tectonics, Sedimentary Basins, and Provenance: A Celebration of the Career of William R. Dickinson* (Vol. Special Paper 540, pp. 547–569). Geological Society of America. https://doi.org/10.1130/2018.2540(24)

Shaw, C. A., Snee, L. W., Selverstone, J., & Jr, J. C. R. (1999). 40Ar/39Ar thermochronology of Mesoproterozoic metamorphism in the Colorado Front Range. *The Journal of Geology*, *107*(1), 49–67. https://doi.org/10.1086/314335

Shuster, D. L., Flowers, R. M., & Farley, K. A. (2006). The influence of natural radiation damage on helium diffusion kinetics in apatite. *Earth and Planetary Science Letters*, *249*(3–4), 148–161. https://doi.org/10.1016/j.epsl.2006.07.028

Siddoway, C. S., & Gehrels, G. E. (2014). Basement-hosted sandstone injectites of Colorado: A vestige of the Neoproterozoic revealed through detrital zircon provenance analysis. *Lithosphere*, *6*(6), 403–408. https://doi.org/10.1130/l390.1

Siddoway, C. S., Myrow, P., & Fitz-Díaz, E. (2013). Strata, structures, and enduring enigmas: A 125th Anniversary appraisal of Colorado Springs geology (pp. 331–356). Geological Society of America. https://doi.org/10.1130/2013.0033(13)

Siddoway, C. S., Palladino, G., Prosser, G., Freedman, D., & Duckworth, W. C. (2019). Basement-hosted sand injectites: use of field examples to advance understanding of hydrocarbon reservoirs in fractured crystalline basement rocks. *Geological Society London Special Publications*, *493*, SP493-2018–140.

Smith, E. F., Nelson, L. L., O'Connell, N., Eyster, A., & Lonsdale, M. C. (2022). The Ediacaran−Cambrian transition in the southern Great Basin, United States. *GSA Bulletin*. https://doi.org/10.1130/b36401.1

Smith, T. M., Saylor, J. E., Lapen, T. J., Leary, R. J., & Sundell, K. E. (2023). Large detrital zircon data set investigation and provenance mapping: Local versus regional and continental sediment sources before, during, and after Ancestral Rocky Mountain deformation. *GSA Bulletin*. https://doi.org/10.1130/b36285.1

Spiegel, C., Kohn, B., Belton, D., Berner, Z., & Gleadow, A. (2009). Apatite (U-Th-Sm)/He thermochronology of rapidly cooled samples: The effect of He implantation. *Earth And Planetary Science Letters*, *285*, 105–114. https://doi.org/10.1016/j.epsl.2009.05.045

Author Manuscript

This article is protected by copyright. All rights reserved.

Stewart, J. H. (1970). *Upper Precambrian and lower Cambrian strata in the southern Great Basin, California and Nevada* (Professional Paper 620) (p. 206). United States Geological Survey.

Sweet, D. E., & Soreghan, G. S. (2010). Late Paleozoic tectonics and paleogeography of the ancestral Front Range: Structural, stratigraphic, and sedimentologic evidence from the Fountain Formation (Manitou Springs, Colorado). *GSA Bulletin*, *122*(3–4), 575–594. https://doi.org/10.1130/b26554.1

Sweet, D. E., Carsrud, C. R., & Watters, A. J. (2015). Proposing an Entirely Pennsylvanian Age for the Fountain Formation through New Lithostratigraphic Correlation along the Front Range. *Mountain Geologist*, *52*(2), 43–70. https://doi.org/10.31582/rmag.mg.52.2.43

Tweto, O. (1979). *MI-16 Geoloigic Map of Colorado* (No. MI–16).

Tweto, O., & Sims, P. K. (1963). Precambrian Ancestry of the Colorado Mineral Belt. *Geological Soceity of America Bulletin*, *74*(8), 991–1014. https://doi.org/10.1130/0016-7606(1963)74[991:paotcm]2.0.co;2

Wang, R., Shen, B., Lang, X., Wen, B., Mitchell, R. N., Ma, H., et al. (2023). A Great late Ediacaran ice age. *National Science Review*, *10*(8), nwad117. https://doi.org/10.1093/nsr/nwad117

Wawrzyniec, T. F., Ault, A. K., Geissman, J. W., Erslev, E. A., & Fankhauser, S. D. (2007). Paleomagnetic dating of fault slip in the Southern Rocky Mountains, USA, and its importance to an integrated Laramide foreland strain field. *Geosphere*, *3*(1), 16–25. https://doi.org/10.1130/ges00066.1

Weil, A. B., & Yonkee, A. (2023). The Laramide orogeny: Current understanding of the structural style, timing, and spatial distribution of the classic foreland thick-skinned tectonic system. In *Laurentia: Turning Points in the Evolution of a Continent* (pp. 707–771). https://doi.org/10.1130/2022.1220(33)

Weimer. (1973). A guide to uppermost Cretaceous stratigraphy, central Front Range, Colorado: deltaic sedimentation, growth faulting and early Laramide crustal movement. *The Mountain Geologist*, *10*(3), 53–97.

Whitmeyer, S. J., & Karlstrom, K. E. (2007). Tectonic model for the Proterozoic growth of North America. *Geosphere*, *3*(4), 220–259. https://doi.org/10.1130/ges00055.1

Wildman, M., Brown, R., Watkins, R., Carter, A., Gleadow, A., & Summerfield, M. (2015). Post break-up tectonic inversion across the southwestern cape of South Africa: New insights from apatite and zircon fission track thermochronometry. *Tectonophysics*, *654*(C), 30–55. https://doi.org/10.1016/j.tecto.2015.04.012

This article is protected by copyright. All rights reserved.

Author Manuscript

Willett, C. D., Fox, M., & Shuster, D. L. (2017). A helium-based model for the effects of radiation damage annealing on helium diffusion kinetics in apatite. *Earth And Planetary Science Letters*, *477*, 1–10. https://doi.org/10.1016/j.epsl.2017.07.047

Wilson, A. B., & Bryant, B. (2006). Isotopic ages of rocks in the northern Front Range, Colorado. *USGS Open-File Report*, (2006–1051).

Witkosky, R., & Wernicke, B. P. (2018). Subsidence history of the Ediacaran Johnnie Formation and related strata of southwest Laurentia: Implications for the age and duration of the Shuram isotopic excursion and animal evolution. *Geosphere*, *14*(5), 2245–2276. https://doi.org/10.1130/ges01678.1

Wrucke, C. T., & Wilson, R. F. (1967). *Geologic map of the Boulder quadrangle, Boulder County, Colorado* (USGS Open-File Report No. 67–281).

Yonkee, W. A., & Weil, A. B. (2015). Tectonic evolution of the Sevier and Laramide belts within the North American Cordillera orogenic system. *Earth Science Reviews*, *150*(C), 531–593. https://doi.org/10.1016/j.earscirev.2015.08.001

Yonkee, W. A., Dehler, C. D., Link, P. K., Balgord, E. A., Keeley, J. A., Hayes, D. S., et al. (2014). Tectono-stratigraphic framework of Neoproterozoic to Cambrian strata, west-central U.S.: Protracted rifting, glaciation, and evolution of the North American Cordilleran margin. *Earth Science Reviews*, *136*(C), 59–95. https://doi.org/10.1016/j.earscirev.2014.05.004

Kluth, C. F., & Coney, P. J. (1981). Plate tectonics of the Ancestral Rocky Mountains. Geology, 9(1), 10–15.

Leary, R. J., Umhoefer, P., Smith, M. E., & Riggs, N. (2017). A three-sided orogen: A new tectonic model for Ancestral Rocky Mountain uplift and basin development. Geology, 45(8), 735–738. https://doi.org/10.1130/g39041.1

Sloss, L. L. (1963). Sequences in the Cratonic Interior of North America. GSA Bulletin, 74(2), 93–114. https://doi.org/10.1130/0016-7606(1963)74[93:sitcio]2.0.co;2

Myrow, P. M., Taylor, J. F., Miller, J. F., Ethington, R. L., Ripperdan, R. L., & Allen, J. (2003). Fallen arches: Dispelling myths concerning Cambrian and Ordovician paleogeography of the Rocky Mountain region. Geological Society of America Bulletin, 115(6), 695–713. https://doi.org/10.1130/0016-7606(2003)115<0695:fadmcc>2.0.co;2

Additional References in Supporting Information

Flowers, R. M., Farley, K. A., & Ketcham, R. A. (2015). A reporting protocol for thermochronologic modeling illustrated with data from the Grand Canyon. *Earth And Planetary Science Letters*, *432*(C), 425–435. https://doi.org/10.1016/j.epsl.2015.09.053

Gehrels, G. E., Valencia, V. A., & Ruiz, J. (2008). Enhanced precision, accuracy, efficiency, and spatial resolution of U-Pb ages by laser ablation-multicollector-inductively coupled plasma-mass spectrometry. *Geochemistry Geophysics Geosystems*, *9*(3), Q03017. https://doi.org/10.1029/2007gc001805

This article is protected by copyright. All rights reserved.

Author Manuscript

Harder, V., Morgan, P., & Swanberg, C. A. (1980). Geothermal resources in the Rio Grande Rift: origins and potential. *Geothermal Resources Council Transactions*, *4*, 61–64.

Kluth, C. F. (1997). Comparison of the Location and Structure of the Late Paleozoic and Late Cretaceous-Early Tertiary Front Range Uplift. In *Colorado Front Range Guidebook* (pp. 31–42). Rocky Mountain Association of Geologists.

Kubati, M. A., Mattash, M. A., Alnethary, M. F., Minissale, A., & Vaselli, O. (2015). Geothermal Exploration and Geothermometric Characteristics of Western Area in Yemen (pp. 1–7). Melbourne, Australia. Retrieved from https://pangea.stanford.edu/ERE/db/WGC/papers/WGC/2015/11008.pdf

Ludwig, K. R. (2008). Isoplot 3.60. *Berkeley Geochronology Center, Special Publication*, 1–77.

Minder, J. R., Mote, P. W., & Lundquist, J. D. (2010). Surface temperature lapse rates over complex terrain: Lessons from the Cascade Mountains. *Journal of Geophysical Research*, *115*(D14), D14122-13. https://doi.org/10.1029/2009jd013493

Pepin, N., & Losleben, M. (2002). Climate change in the Colorado Rocky Mountains: free air versus surface temperature trends. *International Journal of Climatology*, *22*(3), 311–329. https://doi.org/10.1002/joc.740

Reiter, M., Shearer, C., & Edwards, C. L. (1978). Geothermal anomalies along the Rio Grande rift in New Mexico. *Geology*, *6*(2), 85.

Scott, G. R., & Cobban, W. A. (1965). *Geologic and biostratigraphic map of the Pierre Shale between Jarre Creek and Loveland, Colorado*. United States Geological Survey.

Swanberg, C. A. (1983). Geothermal resources of rifts: A comparison of the Rio Grande Rift and the Salton Trough. *Tectonophysics*, *94*(1–4), 659–678.

Weimer, R. J., & Ray, R. R. (1997). Laramide Mountain Flank Deformation and the Golden Fault Zone, Jefferson County, Colorado. In *Colorado Front Range Guidebook* (pp. 49–64). Rocky Mountain Association of Geologists.

Wells, J. D. (1967). *Geology of the Eldorado Springs Quadrangle, Boulder and Jefferson Counties, Colorado*.

Author Manuscript

This article is protected by copyright. All rights reserved.

Table 1. (U-Th)/He Results Summary[a]

	Sample				Apatite He[c]						Zircon He[c]					
Sample	Elev. *(m)*	Latitude	Longitude	Rock[b]	#	Age avg. *(Ma)*	s.d. *(Ma)*	s.d. %	Age range *(Ma)*	[*eU*] range *(ppm)*	#	Age avg. *(Ma)*	s.d. *(Ma)*	s.d %	Age range *(Ma)*	[*eU*] range *(ppm)*
Range Front																
13BC-A*	2256	39.981762	-105.37420	Ppz	4	59	1.9	3%	58-62	35-68	6	59	7.2	12%	50-67	1178-2344
13BC-B*	2454	39.961931	-105.37702	Ppz	4	57	7.1	12%	47-64	2-13	6	–	–	66%	147-607	379-821
13BC-C*	2469	39.98217	-105.38708	Ppz	4	57	3.2	6%	54-60	24-58	6	–	–	30%	62-129	601-1340
13BC-D	2195	39.988535	-105.36926	Ppz	4	59	4.0	7%	56-64	45-83	6	–	–	21%	54-96	778-1634
13BC-E	2057	39.995788	-105.35495	Ppz	4	59	3.9	7%	54-63	28-90	6	69	5.1	7%	65-79	736-1651
13BC-F	1905	40.001652	-105.35234	Ppz	4	54	7.9	15%	42-59	33-96	6	–	–	27%	59-110	631-1788
13BC-G[d]	n/a	n/a	n/a	Ppz	4	57	3.7	7%	53-61	32-86	6	61	7.8	13%	50-74	851-1377
Range Middle																
16NBC-B02	2600	40.02556	-105.42378	Ppz	4	50	1.6	3%	48-52	11-14	6	–	–	19%	47-86	531-1072
16NBC-B01	2728	40.02675	-105.41883	CMB	4	55	8.1	15%	46-65	26-41	0	–	–	–	–	–
16FM-B06	2612	40.04806	-105.46642	CMB	4	48	7.3	15%	41-56	21-33	0	–	–	–	–	–
Divide																
16MBC-B01*	3925	40.01428	-105.63858	Ppz	4	55	2.0	4%	52-57	23-60	6	–	–	18%	73-108	343-921
16MBC-B02	3712	40.01000	-105.64589	Ppz	4	56	2.0	4%	52-57	24-51	6	75	7.1	9%	67-83	289-762
16MBC-B03	3363	40.00617	-105.65086	Ppz	4	39	4.1	11%	35-44	4-24	0	–	–	–	–	–
16MBC-B04*	3254	40.00319	-105.64360	Ppz	4	46	2.4	5%	44-49	11-23	6	72	5.8	8%	66-81	375-865

*sample used in thermal history modeling (Fig. 3)

[a]Data from Murray, Niemi, et al., 2022

[b]Rock type. Ppz—Paleoproterozoic crystalline rock; CMB—Colorado Mineral Belt pluton

[c](U-Th)/He ages reported as an average only for samples with s.d.≤15%, our threshold for instrasample reproducability.

[d]Sample location not recorded, but it was collected close to 13BC-F.

Author Manuscript

This article is protected by copyright. All rights reserved.